INTERACTIONS: SOLAR AND LASER BEAMS IN STRATUS CLOUDS, FRACTALS & MULTIFRACTALS IN CLIMATE & REMOTE-SENSING STUDIES

ANTHONY B. DAVIS,[†] ALEXANDER MARSHAK,[#]
ROBERT F. CAHALAN, and WARREN J. WISCOMBE

NASA's Goddard Space Flight Center, Climate & Radiation Branch
NASA–GSFC (Code 913), Greenbelt, Md 20771, USA

ABSTRACT

Recent research on cloud structure and cloud-radiation interaction at NASA's Goddard Space Flight Center is presented as a show case of interdisciplinary work where fractals and multifractals play a central role. Focus has been primarily on stratocumulus because of their first-order effect on the Earth's energy balance (hence the global climate) due to their unusual horizontal extension and persistence. These cloud layers have quasi-flat upper/lower boundaries and appear to be quite uniform but are highly variable inside. The general strategy has been: utilization of spatial statistics of in situ and remotely sensed *data* pertaining to cloud structure to constrain stochastic cloud *models* used in turn for radiative transfer *simulations* where artificial radiation fields are generated; these fields are compared to actual measurements, and so on, until a degree of closure is achieved. The major trends have been: *i)* computation and understanding of cloud-radiative properties from the large scales of interest to Global Climate Models (over 10^2 km) down to the smallest observable scales (less than 10 m); *ii)* from predicting the outcome of "ideal" measurements to those of "real" ones with limited accuracy, sampling and averaging; *iii)* from passive to active remote-sensing methods; and *iv)* shifting from standard to wavelet-based analysis/modeling techniques. In terms of potential for impact on geophysical research at large, the most important contributions are: *a)* criteria for and measures of nonstationarity and intermittency in scale-invariant data; *b)* so-called "bounded" multifractal cascade models having a continuously variable degree of nonstationarity; *c)* a parameterization of the bulk effect of fractal variability on large-scale planetary albedo; and *d)* the basic scaling theory of radiative "smoothing" that explains non-trivially related multiple scattering phenomena in both solar- and lidar-based remote sensing. The last item also suggests new methods of observing clouds and new ways of processing cloud radiance data to retrieve physical cloud properties.

[†]Soon at: *Los Alamos National Laboratory, Astrophysics & Radiation Measurements Group Los Alamos, NM 87545.*
[#]Soon at: *Joint Center for Earth Systems Technology (JCET), Un. of Maryland – Baltimore County, MD 21228-5398.*
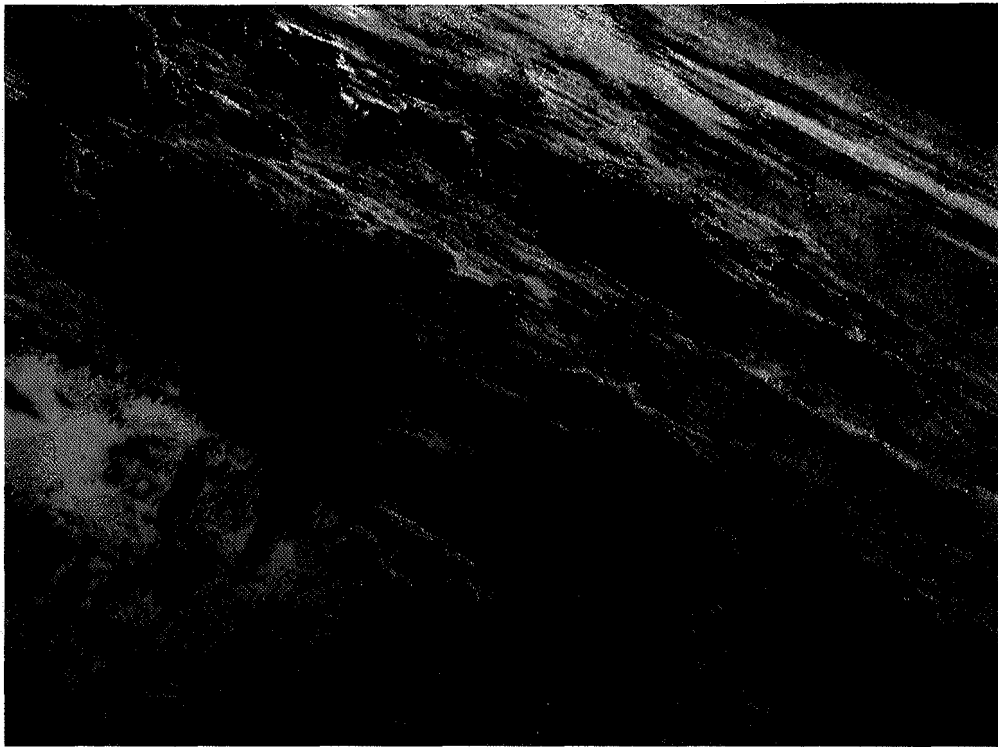
Figure 1a: *Typical Cloud-Scape Captured from the Space Shuttle.* The complexity of this scene should be contrasted with the "standard" cloud model in computational meteorology: an infinitely extended, internally homogeneous (or, at best, stratified) plane-parallel slab. Most of this paper is concerned with the rather bland clouds in the upper r.h. corner: marine stratocumulus (Sc). They are very persistent and horizontally extended, therefore carry considerable weight in the overall reflectance (albedo) of the planet and, from there, command a strong effect on its climate; marine Sc are flat-topped but have huge internal variability, not necessarily apparent to the remote observer.
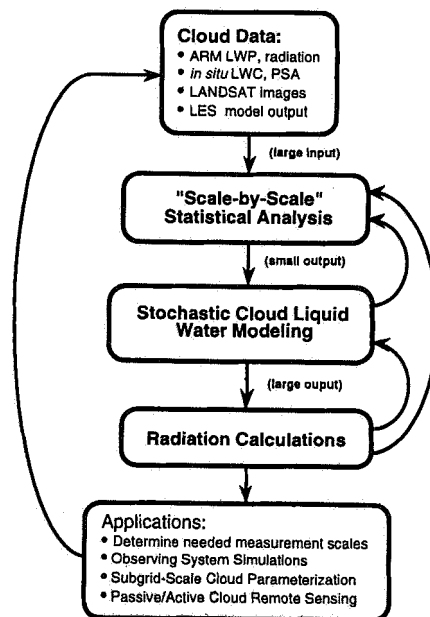

Figure 1b: *Flow-Chart for DoE-Funded Cloud Structure/Radiation Studies at NASA's Goddard Space Flight Center.*

1. INTRODUCTION

1.1 Context: Clouds According to Instrumental and Computational Meteorologies

Clouds have been isolated as one of the major sources of uncertainty in numerical climate prediction, primarily via their interaction with solar and thermal radiation. The most challenging aspect of cloud-radiation interaction is certainly the complex 3D geometry of clouds, cf. Fig. 1a. By cloud "geometry," we mean not only their convoluted shapes, clearly manifestations of the convection, shear, and ensuing turbulence in atmospheric flows; we also have the internalstructure of clouds in mind. Until quite recently, this internal geometry can only be probed with instruments carried by balloons or aircraft that penetrate the cloud layer. Sophisticated remote sensing systems called "millimeter radars" — sensitive not only to (precipitating) rain drops but also (suspended) cloud droplets — will now inform us about the fluctuations in liquid water concentration in the depths of clouds.[1]

Faced with a difficult problem such as cloud structure and evolution, contemporary dynamical meteorology has one of two responses:

- If the problem is deemed relatively "unimportant" with respect the dynamics of interest, it is "parameterized." This is the fate of clouds and/or radiation in a Global Climate Model (GCM) where the finest detail is $\approx 10^2$ km across. Indeed, the particulars of clouds in an individual cell are far too intricate to be described in any kind of detail, and radiation (in the sense of heating/cooling rates) acts too slowly for the computational burden it represents. So, the radiative budget is computed with clouds modeled as infinite homogeneous plane-parallel slabs because analytical solutions exist for the radiative transfer only in this idealized case.

- If, on the contrary, the cloud structure and evolution is perceived as important and interesting, then the computer code is modified so that it can resolve some of the details without sacrificing scales relevant to the meteorologist. This is how "Cloud Ensemble Models" (CEMs, with $\approx 10^{2-3}$ m resolution) and "Large Eddy Simulations" (LESs, $\approx 10^{1-2}$ m resolution) are developed. However, none of the above are able to simulate a cloud as convincingly to the eye as a (sometimes very simple) recursive algorithm and a pseudo-random number generator.

1.2 More Context: Clouds According "Pure" and "Applied" Fractology

The fractal cloud models we have just eluded to, along with closely-related fractal models of natural terrain, have reached over the past two decades a high degree of sophistication. The major players in this arena are R. Voss, S. Lovejoy, and K. Musgrave, all three were collaborators of Prof. Benoit Mandelbrot, in one capacity or another. The interested reader is referred to the respective home-pages[*] of these eclectic individuals for selected biographies (and some stunning fractal vistas); here, we mention only the aspect of their work that has influenced or concurred with ours. Prof. Richard Voss has mastered fractional Brownian motion (fBm) — the prototype of a random monoscaling non-differentiable function — like none other in his "Random Fractal Forgeries;" he was the first to use Fourier-space filtering[2] to obtain fBm without grid effects and semi-transparent textures to simulate clouds, generally embedded in dramatic fractal mountain ranges. Prof. Shaun Lovejoy can be credited with bringing fractals into meteorology through a quantitative analysis of satellite and weather radar data; his seminal 1982 *Science* paper[3] showed

---

[*]Richard F. Voss: http://rs6000.adm.fau.edu/divdept/physics/staff/voss.htm; Shaun M. Lovejoy :
http://www.physics.mcgill.ca/WWW/shaun/; Ken Musgrave: http://www.seas.gwu.edu/faculty/musgrave/index.html

that individual clouds (merged with localized precipitation events) follow a non-trivial area-perimeter law. In collaboration with Dr. Daniel Schertzer of Météo-France, Prof. Lovejoy has since been applying multifractal concepts to atmospheric phenomena, using hydrology (where multifractal ideas have gained more acceptance[4]) as a stepping stone. Prof. Kenneth Musgrave has recently pushed the envelop of fractal computer art into new heights (including animation) with his "Slartibardfarst[†] System" which is based on iterated products of localized functions,[5] an idea that naturally leads to random multifractal fields (cf. §3.1).

Fifteen years after Lovejoy's landmark paper, fractal cloud models are only beginning to gain credence in mainstream meteorology. The reasons for this lag are easy to understand:

• The most meteorologically-incorrect feature of fractal clouds is that they have essentially "parameterized" the dynamics: thay are contained in the recursion rules that generate the new small-scale structures, as if by nonlinear instability and break-up of the larger ones.

• Furthermore, fractal cloud models have no "cloud microphysics" (terminology designating the thermodynamical considerations that tell cloud-physicists how clouds form via condensation).

• Finally, fractal clouds are not usually subject to the laws of atmospheric optics: the computer artist's false-color palette adds the final touch to these often very convincing renderings of what Baudelaire[6] called '*those moving architectures that God builds out of vapors, wonderful constructions of the intangible.*'

Objections to fractal cloud modeling in the above list — no fluid dynamics, no thermal physics, and no optics — are akin to those voiced against fractals in general early on. At any rate, the last was the first to be addressed by using fractals and multifractals as *ad hoc* cloud models in the sense of scattering/absorbing media in radiative transfer computations. This is primarily[#] work of the "Montreal/Paris" group (coordinated by Shaun Lovejoy and Daniel Schertzer) and of the "Goddard" group (spearheaded by the two last of the present co-authors). The remaining lack of thermo- and hydrodynamical justification is addressed empirically by requiring the cloud models to have the same type of variability observed in real clouds. This notion of "same type of variability" is made precise by using spatial statistics of course, but this introduces a large degree of freedom-of-choice. So it is no surprise that the two groups have followed diverging paths.[*] This review covers the fractal/cloud/radiation work performed at NASA's Goddard Space Flight Center over the past five years or so. Instead of addressing right away the other two "standard-objections-to-fractal-cloud-models," the drive has been to identify practical meteorological issues that can only be solved with fractal tools or, at least, are most elegantly solved with fractals.

1.3 Outline

Figure 1b shows schematically how our group operates on three tiers — statistical data analysis, stochastic cloud modeling, radiation transport computations — and this provides a convenient template for this review. (However, the activities are conducted more often in parallel than in sequence which is the intended meaning of the feed-back loops.) In section 2, we explain in some detail our perspective on geophysical data analysis in general; it hinges on precise operational definitions of statistical stationarity and intermittency (cloud data is used here for illustration). In

---

[†]Character in Douglas Adams' "The Hitch-hiker's Guide to the Galaxy" that created Earth's topography.

[#]Also noteworthy are the contributions of Dr. H. Barker of the Atmospheric Environment Service (Canada) and Prof. K. F. Evans of the University of Colorado's Program in Atmospheric & Oceanic Sciences (Boulder, CO).

[*]By-and-large, the strategy of the Montreal/Paris group seems to be the cumulation of applications of their specific data analysis methods and closely related multifractal models. Currently, their interests range from earthquakes to the large-scale structure of the Universe; the interested reader is referred to a forthcoming monograph.[92]

section 3 we describe two multifractal cloud models that we have found useful, as cloud surrogates in radiation studies, as tutorial- and calibration tools in data analysis exercises, or both. In section 4 we survey our investigations of the solar illumination problem in realistically variable cloud models by sorting out our findings between large- and small scales, reflectance and absorptance. Section 5 shows how radiative Green functions and photon diffusion theory explain some surprising observations, then lead to new ideas in cloud lidar instrumentation. Finally, in section 6 we list our achievements in a classification by category, outline future work, and discuss the feed-back of fractal cloud studies into fractal science at large.

2. SCALE-BY-SCALE DATA ANALYSIS, ILLUSTRATED WITH CLOUD LIQUID WATER CONTENT

2.1 Spectral Analysis: Results from a New Instrument

The most preliminary analysis of a complex signal or image usually consists in compiling 1-point statistics such as mean and variance, sometimes a histogram, and often a wavenumber spectrum $E(k)$; the latter is sometimes converted into a 2-point auto-covariance function via inverse Fast Fourier Transform (FFT). Fourier space is a natural environment for variability analysis: $k = 0$ yields the spatial mean, and $k = |k| > 0$ gives a scale-by-scale breakdown of the variance. In large geophysical systems, we generally have to deal with a considerable range of scales and high levels of variability. So we are soon looking at log-log plots and seeking "scale-invariance," i.e., straight lines that indicate power-law behavior with respect to a scale parameter. For instance, with $E(k)$ and wavenumber k, we look for regimes where

$$E(k) \sim k^{-\beta}. \tag{1}$$

Figure 2 shows a 24-km horizontal transect of the density of the liquid water (known as "liquid water content," or LWC, in g/m^3) inside a marine boundary layer cloud system sampled at 4-cm resolution, which has become possible only quite recently.[7] The wavenumber spectra in Fig. 3 are patently *not* scale-invariant, showing a scale-break at $r = 1/k \approx 2$–5 m:

- The broad fluctuations in the large-scale regime, Fig. 2a, have been documented previously[8–10] and have $\beta \approx 1.4$–1.6 in Eq. (1), which is characteristic of turbulent signal. Although not at all a passive scalar, water vapor and cloud droplets are advected by atmospheric motions.
- The sharp positive fluctuations in the small-scale regime, Fig. 2b, have never been observed directly before.[11] However, we hold them responsible for the previously observed[12] deviations from Poissonian behavior in the record of droplet arrival times as a tiny laser beam sweeps through cloudy air. In this regime, we have $\beta \approx 0.9$.

The physical mechanism that produces the strong spikes in Fig. 2b is not well-understood at present but is probably related to stretching-and-folding at the interface of moist and dry air masses in the cloud. In sharp contrast to this, the low-level background noise is readily traceable to instrumental characteristics; being white ($\beta = 0$), this noise does not explain the scale-break (more details in ref. [11]).

Mathematically, the spectrum in Fig. 3 contains a double paradox: the large-scale law in $\beta > 1$ requires a cut-off at some "integral" scale to avoid an infra-red divergence of total variance; the small-scale law in $\beta < 1$ needs a cut-off to ensure convergence in the (ultraviolet) limit $k \to \infty$. The existence of an integral scale — hence another scale-break — can be argued on physical
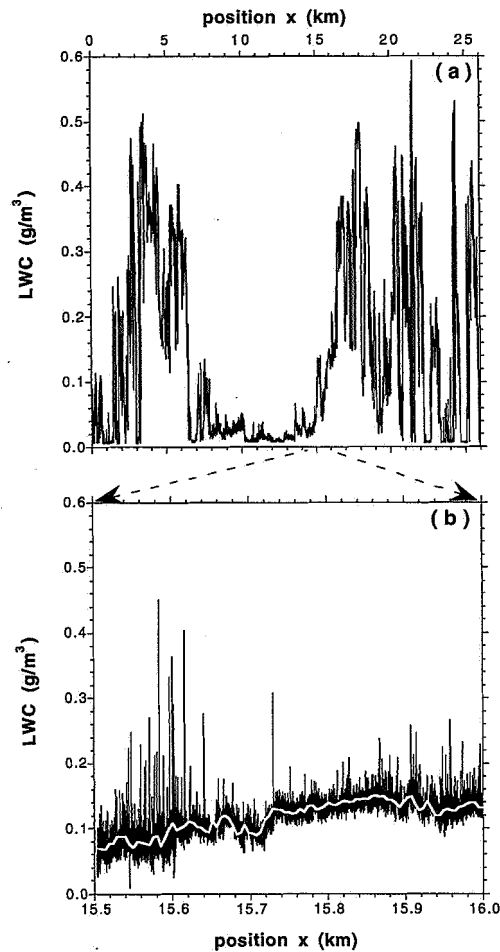
Figure 2: *Cloud Liquid Water Content (LWC) from a Research Aircraft Penetration.* This particularly long (24 km) and detailed (4-cm resolution) look at internal cloud structure was obtained on 07/26/93 during the winter-season Southern Ocean-Cloud EXperiment, SOCEX–1, conducted off the coast of Tasmania. (a) Large-scale structure, as represented by 5-m averages. (b) Small-scale structure, a typical sample.
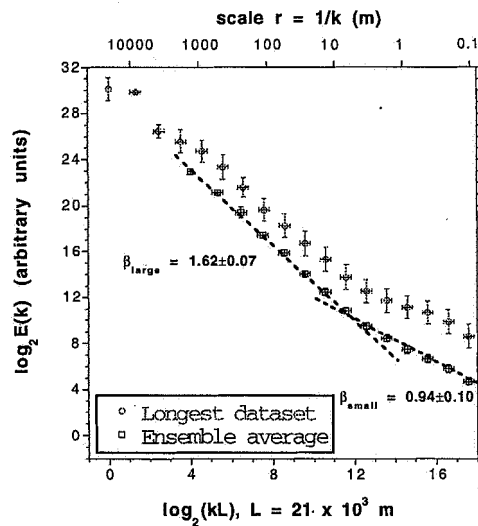

Figure 3: *Wavenumber Spectra of Cloud LWC.* $E(k)$ on a log-log plot for the dataset described in Fig. 2, as well as for the whole SOCEX database that contains several shorter datasets.[11]

grounds as well: LWC is a non-negative quantity, so the amplitudes of its Fourier modes cannot increase indefinitely beyond the value of its mean (otherwise, negative values would be generated somewhere). Physical considerations also resolve the small-scale problem, without a new scale-break this time: LWC simply loses its meaning as a continuum quantity as the scale of interest $(r = 1/k)$ approaches the characteristic inter-droplet distance $n^{-1/3}$. Droplet density n is highly variable in space and time, although not as much as LWC; a typical value is $100/cm^3$.

2.2 Ramifications of Scale-Invariance in Fourier Space

Spectral analysis has been heavily criticized — most recently by the wavelet community — for its inability to capture unambiguously strongly localized events. Indeed, a Heaviside step-function and Brownian motion (the running sum of many random steps) have spectra with k^{-2} scaling. This lack of discrimination is a serious hindrance in modeling, of cloud structure in particular, but has not yet deterred many practitioners from applying spectral analysis liberally.

We also believe spectral analysis is still a good starting point for most applications. We say this not only because it is well-accepted and innocuous: in conjunction with scale-invariance, spectral analysis gains meaning and can be assigned a specific task in data analysis.[9,13] Following a path open by Benoit Mandelbrot,[14] we invoked the Wiener-Khinchin theorem for statistically stationary processes[a] that are also scale-invariant[b] to show that $\beta < 1$ means (broad-sense) stationarity and $\beta > 1$ nonstationarity, $\beta < 3$ implies stationary increments, and so on. This is probably the simplest test for stationarity in real data, an important piece of information because many popular statistics are designed for stationary processes and will give meaningless results if applied to nonstationary data. For instance, a running mean does not converge in a nonstationary regime.

Scale-invariance is a such strong constraint on a random process that along with the statistical information about its stationarity (or lack of) comes analytical information,[c] as well as geometrical information about its graph.[d] Indeed, a stationary scale-invariant process ($\beta < 1$) is almost everywhere discontinuous and its graph is space-filling; a nonstationary scale-invariant process with stationary increments ($1 < \beta < 3$) is almost everywhere continuous (which does not exclude isolated jumps, as in a Heaviside step) and its graph has a generally non-trivial graph dimension.

The fundamental issue here is correlation range. Conventional wisdom is that scale-invariant processes have "long-range" correlations. This is true but has rather different meanings for stationary and nonstationary situations,[13] both of which are present in Figs. 2–3:

- Correlations are the longest in the nonstationary ($\beta > 1$) case, so ubiquitous in nature: because of the stochastic continuity, most jumps are small, and large differences (a necessary condition for decorrelation) can only build up over very large scales. In other words, small-scale variance is finite, large-scale variance is not. In more pragmatic terms, this means that the (spurious)

[a] If the random process $f(x)$ is broad-sense stationary, then its auto-covariance function $\langle [f(x+r)-\langle f(x+r)\rangle][f(x)-\langle f(x)\rangle]\rangle$ depends only on the lag r; call it $G(r)$. Furthermore (Wiener-Khinchin theorem), $G(r)$ is in Fourier duality with $E(k)$.

[b] If $f(x)$ is broad-sense stationary, with vanishing mean, and scale-invariant, then its auto-covariance, $G(r) = \langle f(x+r)f(x)\rangle$ is power-law in r: $G(r) \sim r^{-\mu}$, $\mu > 0$; to be (Wiener-Khinchin) equivalent to Eq. (1), this requires $\beta = 1-\mu < 1$.

[c] The 2nd-order structure function $D(r) = \langle [f(x+r)-f(x)]^2 \rangle$ can be used to measure continuity (in the L_2 norm): we require $D(0^+) = \lim_{r\to 0} D(r) = 0$ for $f(\cdot)$ to be stochastically continuous. If $f(\cdot)$ is non-stationary and scale-invariant with $1 < \beta < 3$ (stationary increments), then[14,39] $D(r) \sim r^{\beta-1}$, hence stochastic continuity. On the other side, if $f(\cdot)$ is stationary, then $D(r) = 2[G(0)-G(r)]$ which is ill-defined at $r = 0$ for scale-invariant $f(\cdot)$ since auto-covariance $G(r)$ will be some non-trivial power-law; therefore, scaling and stationarity implies stochastic discontinuity.

[d] The global Hurst exponent H_1 in $\langle |f(x+r)-f(x)|\rangle \sim r^{H_1}$ is related to the graph's (capacity) dimension $D_g = 2-H_1$ for a 1D signal and, generally speaking, H_1 is the graph's co-dimension. Multifractal considerations for nonstationary cases ($1 < \beta < 3$) lead to $H_1 \geq H_2 = (\beta-1)/2$, hence $D_g \leq (5-\beta)/2$, with "=" only for monoscaling processes such as fBm.

integral correlation length of a nonstationary dataset is commensurate with its outer scale which, for all practical purposes, defines the infra-red spectral cut-off. Turning to the "large-scale" cloud structure illustrated in Fig. 2a, it is unlikely to see a running mean of LWC converge over this type of data-stream, its oscillations are basically too broad.

• In the stationary ($\beta < 1$) case, correlations are only long with respect to the inner scale (or pixel-scale) of the data. Because large-scale variance is finite and thanks to the rapid small-scale oscillations, running means converge rather quickly. So the relevant scale to measure correlation length is no longer the outer scale but the pixel scale which controls the ultra-violet cut-off in Fourier space at the Nyquist frequency. In Fig. 2b, running means of LWC over the strong "small-scale" fluctuations — big (physical) and small (instrumental) jumps combined — converge to the relevant "large-scale" value, the slowly varying function plotted in overlay.

2.3 Beyond Spectral Analysis: Two Flavors of Multifractal Analysis

In retrospect, we have followed the historical development of statistical fluid dynamics. After spectral analysis (and closely related 2nd-order structure functions) of the turbulent velocity field:

• first higher-order structure functions[15] were used, eventually in conjunction with the multifractal formalism of Frisch and Parisi,[16]

• then, benefiting from developments in deterministic chaos[†] theory, singularity analysis of the (rate of kinetic energy) dissipation field[20] became popular.

Motivation was to understand the (still actively researched) role of intermittency in turbulence.

If $f(x)$ represents a 1D scale-invariant signal and r is the scale of interest, its qth-order structure function (absolute moment of the increment over r) is expected to be power-law in r, i.e.,

$$\langle |f(x+r)-f(x)|^q \rangle \sim r^{\zeta(q)}, \tag{2}$$

where $\langle \cdot \rangle$ means spatial/ensemble average (resp. over x and f). The family of exponents $\zeta(q)$ has some well-known and/or predetermined members with constraints on their numerical values:

• $\zeta(0) = 0$ (by normalization of r-dependent PDFs of the increments);

• $\zeta(1) = H_1 \in [0,1]$ is the (global) Hurst exponent;[*]

• $\zeta(2) = 2H_2$ determines the scaling of $E(k)$ in Eq. (1) for regimes where $1 < \beta = 2H_2+1 < 3$.

Also, if $f(x)$ happens to be turbulent velocity, Navier-Stokes equations require[23] $\zeta(3) = 3H_3 = 1$.

As a function of a real variable, $\zeta(q)$ has general analytical properties, conditional that there is negligible q-dependence in the prefactors of the generalized scaling law in Eq. (2). Specifically:

• $\zeta(q)$ is concave[16] ($\zeta''(q) \le 0$), equivalently, we can define the non-increasing hierarchy[24]

$$H_q = \frac{\zeta(q)}{q} ; \tag{3}$$

[†]Specifically, generalized dimensions of strange attractors[17-18] and multifractal structure of the invariant measure.[19]

[*]The 1st-order structure function has implicitly been used in numerous geometrical studies since[21] $D_g = 2-H_1$ is the fractal (capacity) dimension of the graph $\{x, f(x)\}$. There has been a renewed interest in it with the relatively recent introduction of the so-called "cancellation" exponent[22] $\kappa = 1-H_1$,

- if furthermore $\langle |f(x+r)-f(x)|^q \rangle < \infty$ in Eq. (2), then $\zeta(q)$ is non-decreasing[25-26] ($\zeta'(q) \geq 0$).

If $\zeta(q) \propto q$, equivalently, if $H_q \equiv constant$, then $f(\cdot)$ is a monofractal process (e.g., fBm); if not, $f(\cdot)$ is a multifractal one.

Figure 4a shows $\langle |f(x+r)-f(x)|^q \rangle$ for the LWC data in Fig. 2 combined with more data from the same flight during SOCEX-1 field program; Fig. 4b shows $\zeta(q)$ for the large-scale regime ($r \geq 5$ m) of our SOCEX database and two other field experiments on marine boundary-layer cloud systems (FIRE and ASTEX). The $\zeta(q)$ are determined (by linear log-log regressions) for r between 5 m and 660 m, so that even the smallest SOCEX dataset is incorporated; however, based on the spectral scaling of the longest un-interrupted flight-segment (cf. Fig. 3), these $\zeta(q)$'s are representative of scales up to 5 km at least. We see that the large-scale structure of these clouds is strongly multifractal. The small-scale ($r \leq 2$ m) regime is stationary which, in principle, means[#] $\zeta(q) \equiv 0$; in practice, it is hard to see scaling at all for a reasonable range in q and we find, at best, spuriously non-vanishing $\zeta(q)$'s (see ref. [11] for details).

In the course of investigating cloud structure and in most other endeavors using geophysical data, we do not have the guidance of a full set of nonlinear equations (such as Navier-Stokes for turbulence) nor a specific phenomenology (such as the idea of a turbulent energy cascade in highly turbulent flows). We can nevertheless always obtain a non-negative stationary "dissipation" field for a given nonstationary signal by taking absolute small-scale gradients; this defines the basic input for a singularity analysis procedure. Let

$$\varepsilon(x) = |f(x+\ell)-f(x)|^m. \tag{4}$$

The natural choices are $m = 2$ and $\ell = \eta$ (Kolmogorov dissipation scale) if f is turbulent velocity. We have generally used $m = 1$, for simplicity; other authors vary m continuously.[27] Unless there is a clear choice (as is the case for the LWC data in Fig. 2), the choice of ℓ needs to be tested for its robustness (since we do not want exponents to depend on an essentially instrumental parameter). Having defined a measure in Eq. (4), we can form the "partition functions"

$$Z(q;r) = \sum_{\{x;\ \text{disjoint "}r\text{-boxes"}\}} [\int_x^{x+r} \varepsilon(x')dx']^q. \tag{5a}$$

These quantities scale as

$$\langle Z(q;r) \rangle \sim r^{\tau(q)}, \tag{5b}$$

where the ensemble-average is based on the shortest dataset (if necessary, longer ones are subdivided into realizations). As for $\zeta(q)$, the exponents $\tau(q)$ have some general properties:[17-19]

- $-\tau(0^+) = D_0 \leq 1$ is the fractal dimension of the support of $\varepsilon(x)$;
- $\tau(1) = 0$, and $\tau'(1) = D_1$ is the "information" dimension of the measure $\varepsilon(x)$;
- $\tau(2) = D_2$, the "correlation" dimension, determines the scaling of $E_\varepsilon(k)$ in Eq. (1) ($\beta_\varepsilon = D_2$).

We also have $\tau''(q) \leq 0$, equivalently, we can define the non-increasing hierarchy

$$D_q = \frac{\tau(q)}{q-1}. \tag{6}$$

[#]Structure functions in Eq. (2) are not only scale-invariant but scale-independent if $f(x+r)$ is decorrelated from $f(x)$.[13,26]
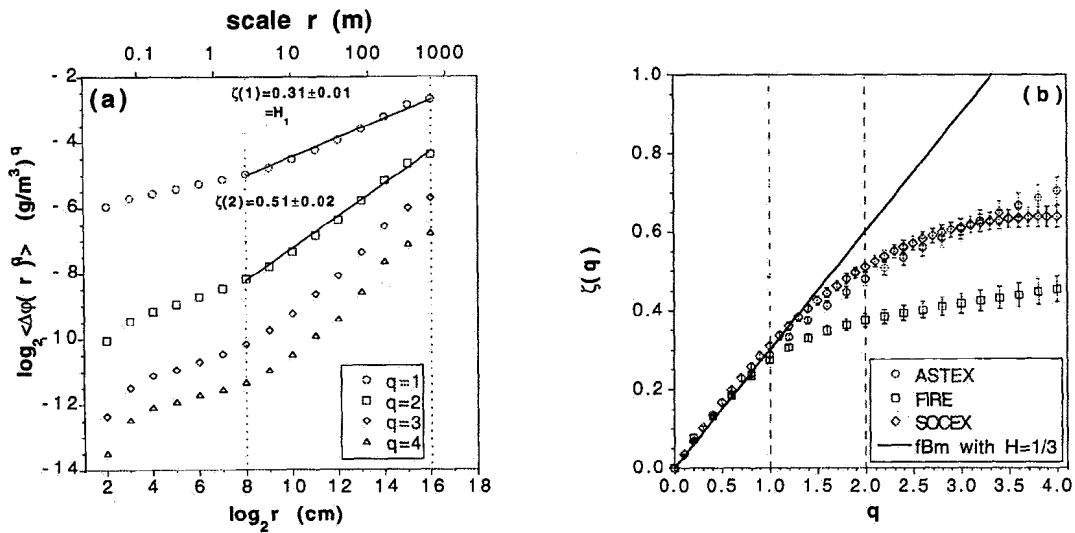
Figure 4: *Structure-Function Analysis of Cloud LWC.* (a) qth-order structure functions for all scales r accessible even with the smallest flight segment from our SOCEX database, and (b) $\zeta(q)$ exponents for the large-scale regime ($r \geq 5$ m); also shown are a monofractal model (e.g., fBm) and two other field programs, briefly described in the caption of Table 1. The more important exponents are highlighted: $H_1 = \zeta(1)$, and $\zeta(2) = \beta - 1$ (cf. Fig. 3 for an independent verification).
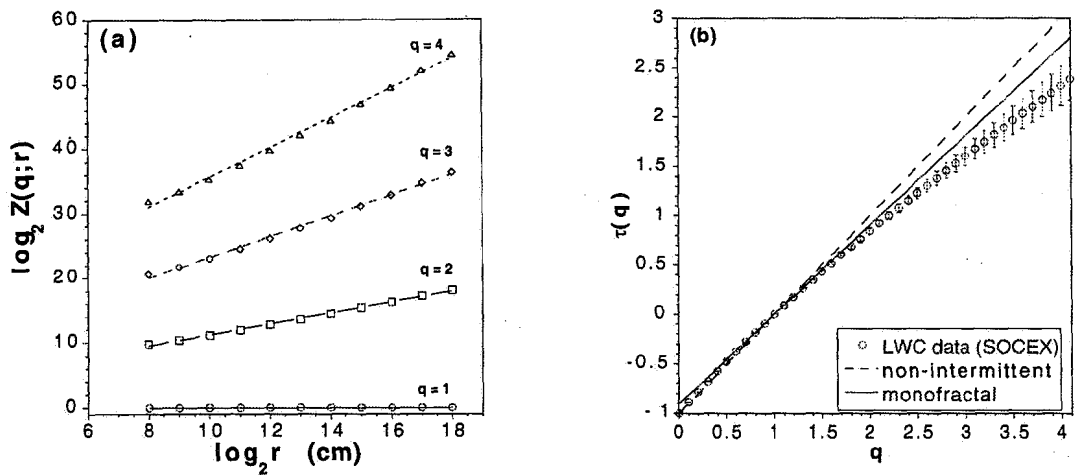

Figure 5: *Singularity Analysis of Large-Scale LWC Variability.* (a) Scaling of partition functions $Z(q;r)$ for measures based on 5-m (next-neighbor) absolute gradients of the large-scale fields such as in Fig. 3a. (b) $\tau(q)$ exponents for the results in panel (a), with non-intermittent ($C_1 = 0$) and monofractal (same C_1) cases for comparison.

For the cloud LWC data in Fig. 2, we take $\ell = 5$ m and $m = 1$ in Eq. (4) after coarse-graining the data to scale ℓ; this amounts to taking next-neighbor differences in Fig. 2a. Figure 5 shows the scaling of the partition functions $Z(q;r)$ in Eq. (5a) and the exponents $\tau(q)$ defined in Eq. (5b). The characteristic curvature of $\tau(q)$ is another statement of the definite multifractality of cloud structure over almost three decades in scale, starting at 2–5 m. An extensive survey of the physics literature[28] shows that this range is close to the upper end of the distribution of scaling ranges used in fractal analyses. The same study shows that claims of "fractality" using one decade or less in scale — a rather frequent occurrence — need to be re-examined. Indeed, such a fractality can be explained generically as a by-product of the data analysis methodology, as opposed to a physical property of the observed system. We now show that claims of "multifractality" should also be scrutinized, especially when the scaling range is small.

2.4 Beyond Multifractal Analysis: Questioning its Robustness

Both $\tau(q)$ and $\zeta(q)-1$ have well-documented Legendre transforms: respectively,[19]

$$F(\alpha) = \min_{q}[\alpha q - \tau(q)] \tag{7}$$

and[16]

$$D(h) = \min_{q}[hq - \zeta(q)] + 1; \tag{8}$$

both of the above are known as "singularity spectra." Interpreted as fractal dimensions, they represent the relative frequencies of occurrence of local orders-of-singularity, $\alpha(x)$, for random measures $\varepsilon(x)$ and Hölder exponents, $h(x)$, for non-differentiable functions $f(x)$. These measures of singularity strength are often bounded by 0 and 1 (and sometimes less) *but not always*. Muzy *et al.*[29] have critiqued both structure functions in Eq. (2) and the so-called "box-counting" methodology set forth in Eqs. (5a–b) because they cannot access singularity strengths outside of this limited range; worse, they yield spurious scaling for large (positive or negative) values of q if there are h's (respectively, α's) outside of the preset bounds. These authors propose wavelet-based methods that not only avoid these pitfalls but unify structure-function and singularity analyses under a single formalism.

The important message for data analysis in the Legendre transforms of $\zeta(q)$ and $\tau(q)$ is that multifractality is traceable to the *non*-degeneracy of the distribution of the local singularity strengths (respectively h's and α's) in the data. However, it is clearly impossible to establish degeneracy with a finite amount of random data sample from an infinite probability space. For instance, a finite sample of fBm — which has $\zeta(q) = qH_1$ in theory — at finite resolution will always yield numerically a nonlinear $\zeta(q)$ since Eq. (2) reads as a finite sum of exponentials of q. Consequently, instead of $D(h) = 1$ for $h = H_1$ (and formally $-\infty$ otherwise), a finite range of h's with non-trivial $D(h)$'s is obtained from the numerical Legendre transform. This spurious multifractality depends critically on the sample size and resolution, in other words instrumental characteristics. Moreover, the observed nonlinearity of $\tau(q)$ will be more pronounced if large values of $|q|$ are investigated since these are Legendre-mapped to the largest or smallest jumps in the data. By definition, these events are operationally sub-sampled in any finite amount of data. Their rarity is a manifestation of a *lack of ergodicity* in the data, not to be confused with the physical concept of intermittency.[4,32]

In summary, it is not enough to say that '*such-and-such data is found to be multifractal*'. At the very least, the r-range and q-range involved must be clearly stated; ideally, a comparison with the same amount of artificial data (or more) with known mono- or multifractal properties is in

order, e.g., refs. [26,30–31]. We have argued[32] that the quantity $[H_{q_{min}}-H_{q_{max}}]\times\log_{10}(r_{max}/r_{min})$ can be used to establish *bone fide* (or, conversely, detect spurious) multifractality in qth-order structure functions, at least in comparative studies: the bigger (smaller) it is, better the chance the data is truly (not) multifractal.[#] The q-range used here must of course not be affected by the severe sampling problems mentioned above. Similar arguments for singularity analysis make use of a previously un-exploited exponent hierarchy, defined at $q = 0$, rather than $q = 1$ as in Eq. (6):

$$X_q = \frac{\tau(q)-\tau(0^+)}{q},$$ (9)

which is also non-increasing; ultimately, it is required that $[X_{q_{min}}-X_{q_{max}}]\times\log_{10}(r_{max}/r_{min})$ be as large (small) as possible to establish (dismiss) true multifractality.[*]

The above "test quantities" are $\log_{10}$'s of the *a priori* extrapolation errors when predicting either $\langle|f(x+r_{max})-f(x)|^{q_{max}}\rangle$ from $\langle|f(x+r_{min})-f(x)|^{q_{min}}\rangle$ and $\zeta(q)$, or $Z(q_{max};r_{max})$ from $Z(q_{min};r_{min})$ and $\tau(q)$, assuming monofractal models for the data.[32]   Small extrapolation errors mean that we can probably use a monofractal model, that the multifractality in the data, if real, is too weak to be distinguished from spurious multifractality. It is clear from Figs. 4b and 5b that the large-scale cloud data in Fig. 2a passes both multifractality tests, more details in ref. [11].

2.5 Simplified, Non-Redundant and Robust Multifractal Analysis in the "Bi-Fractal" Plane

In our effort to go beyond spectral analysis and the associated single-exponent characterization of scale-invariant data, we have collected two complete families of exponents. There is no doubt that both $\zeta(q)$ and $\tau(q)$ capture two different manifestations of the same physical phenomenon known as intermittency. Accordingly, there have been attempts at connecting the two exponent functions. Starting as usual in the realm of statistical turbulence theory, Kolmogorov[33] and Obuhkov[34] determined "intermittency corrections" to the earlier[23] prediction, $\zeta(q) = q/3$, based on a homogeneous dissipation field $\varepsilon(x) \equiv \langle\varepsilon\rangle$, hence $\tau(q) = q-1$. If the energy dissipation field $\varepsilon(x)$ is strongly intermittent, then dimensional analysis (namely,[39] $[v(x+r)-v(x)]^q \sim \varepsilon_r(x)^{q/3}r^{q/3}$ where subscript "r" means averaged to scale r) argues for an correction to $\zeta(q)$ which then reads as $q/3+[\tau(q/3)-(q/3-1)]$; this correction term vanishes, as required, at $q = 0$ and $q = 3$.

A reasonable generalization of the Kolmogorov relation used in turbulence is[35]

$$\langle[f(x+r)-f(x)]^q\rangle \sim \langle\varepsilon_r(x)^{q/b}\rangle \times r^{q/a},$$ (10a)

where $a > 0$ and b is arbitrary (as long as the moments of ε_r used in Eq. (10a) exist); this leads to

$$\zeta(q) = q/a + [\tau(q/b)-(q/b-1)]$$ (10b)

via Eqs. (2) and (5a–b); by this definition, the special case $a = b = 3$ applies to turbulence. Physical justification of such relations is discussed elsewhere.[36] At any rate, one new parameter at least is needed to obtain $\zeta(q)$ from $\tau(q)$ simply because there are two predetermined values for the latter, only one for the former. If Eq. (10b) is true, we can assign this role to the Hurst exponent $H_1 = \zeta(1)$ — which has a simple geometrical meaning (related to the graph dimension) — and do away with one of the two multifractal analysis procedures altogether.

[#]This criterion for spurious multifractality can be adapted into one for spurious nonstationarity, see ref. [11] for details.

[*]Note that, without the $\tau(0^+)$ term in Eq. (9), we obtain a criterion for/against intermittency, rather than multifractality, in data: monofractal intermittent processes (e.g., "β-models" in turbulence) pass the test since $\tau(q) = (q-1)D_0$, $q > 0$.

There are many reasons for wanting to characterize complex data with the smallest number of exponents. Not the least is that when we proceed to generate data with convincingly similar behavior using a stochastic model rather than an instrument, the smaller the number of parameters in the model, the more spectacular the result. We certainly need more than one parameter, because of the ambiguity of stand-alone spectral analysis, but do we need an infinity (the generic multifractal answer)? Furthermore, we have emphasized the difficulty of obtaining reliable estimates, hence exponents, for higher-order moments in a multifractal approach. This argues for using well-selected low-order exponents.

Stationary scale-invariant processes have $\zeta(q) \equiv 0$; so

$$H_1 = \zeta(1) \tag{11}$$

is clearly a 1st-order quantifier of the nonstationarity in data, and the rest of the structure-function exponents merely qualify the nonstationarity. First qualitative question to address: Is the nonstationarity of the monofractal (fBm) kind, or some multifractal kind? Equivalently: Is there intermittency in the system or not? The natural counterpart of Eq. (11) for singularity analysis is

$$C_1 = 1-D_1 = 1-\tau'(1). \tag{12a}$$

From Eqs. (8) and (12a), it is clear that C_1 is the information co-dimension of measure $\varepsilon(x)$ in Eq. (4). If we forego singularity analysis and adopt the $\tau(q)$-to-$\zeta(q)$ connection in Eqs. (10a–b),then

$$C_1 = \zeta(b)-b\zeta'(b), \tag{12b}$$

where parameter b is defined in Eq. (10a). Equation (12b) is clearly a direct measure of the deviation of $\zeta(q)$ from a linear function going through the origin.

We call "bi-fractal analysis" the restricted but non-redundant/robust multifractal analysis limited to H_1 and C_1 determination.[*] These exponents have simple meanings:

- In terms more geometrical than statistical: where H_1 is the codimension of $f(x)$'s rough graph — actually,[21] in any number d of dimensions — C_1 is the codimension of the (generally) sparse subset of space where the local order-of-singularity "$\alpha(x)$" of $\varepsilon(x)$ is $\alpha_1 = d-C_1$, the one that dominates the mean measure $\langle \varepsilon \rangle$ (see ref. [19]).
- In terms more statistical than geometrical: where H_1 quantifies nonstationarity, C_1 quantifies intermittency, leaving the remainder of the $\tau(q)$ exponents to qualify it.

In spite of its obvious limitations, bi-fractal analysis has proved to be a useful diagnostic in our cloud studies. For instance, Fig. 6 shows how standard scale-invariant models live on the boundaries of the accessible (H_1, C_1) domain but geophysical data, including turbulent signals (e.g., velocity and passive scalar density), live inside. This emphasizes the need for new multifractal models, with simultaneously tunable degrees of nonstationarity and intermittency; the handful that we are aware of are surveyed in refs: [10,32].

In Fig. 6 we use the $m = 2$ convention in Eq. (4) to facilitate comparison with turbulence; we see that cloud LWC has similar bi-fractal properties to turbulent velocity; not a surprise in view of the turbulent nature of atmospheric dynamics. In Table 1 we return to the $m = 1$ convention and display (H_1, C_1)-entries for cloud data from a variety of sources. A few remarks are in order:

---

[*]Alternate approaches with a small number of multifractal parameters are in [35,37] and compared to ours in [10].
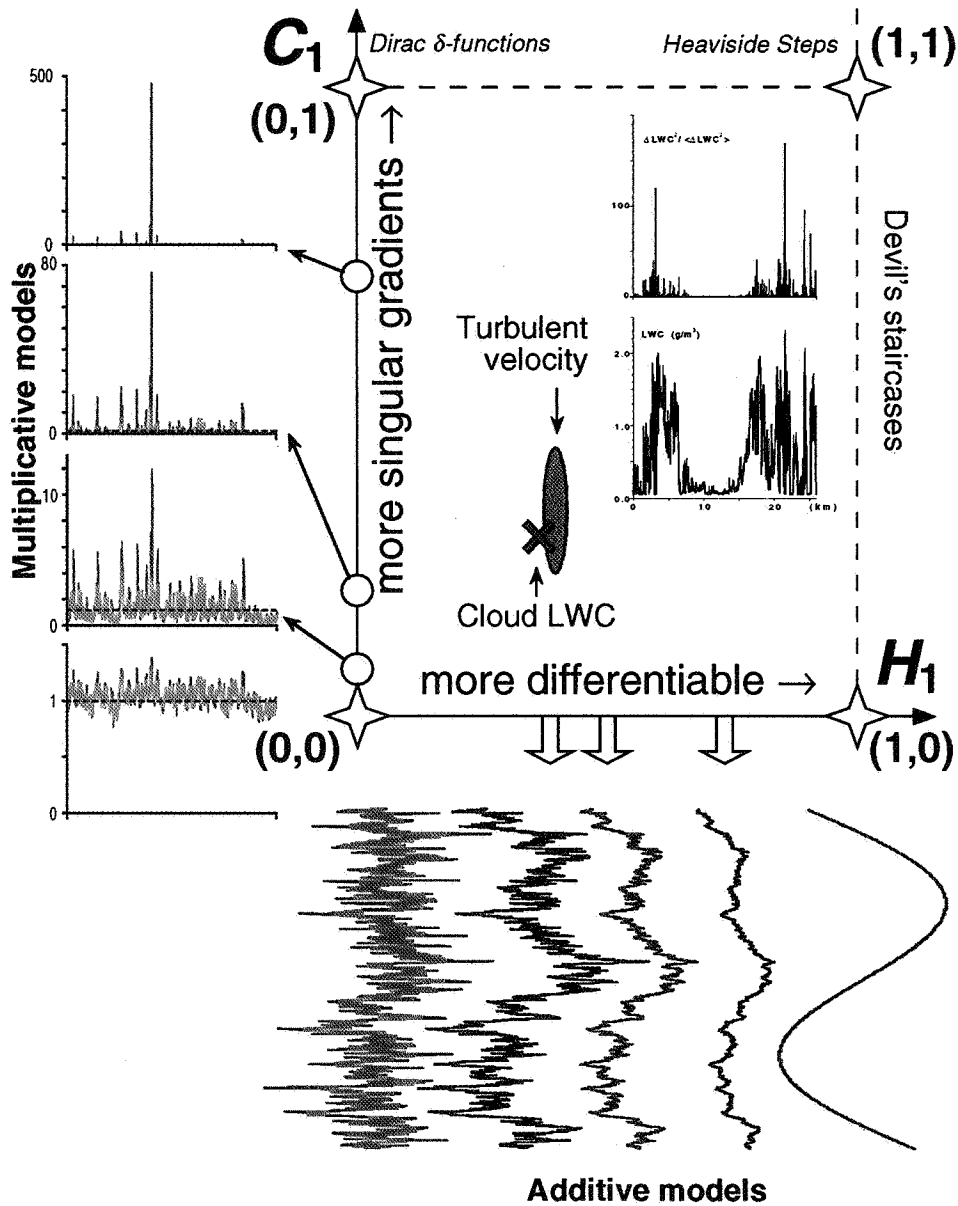
Figure 6: *Bi-Fractal Plane.* The horizontal coordinate is the global Hurst exponent H_1 of the geophysical signal; the vertical coordinate is the information codimension C_1 of the absolute small-scale gradient field. The signal's differentiability (hence graph smoothness) and statistical *non*stationarity increases horizontally, as illustrated by the fBm samples at $H_1 = 1/3$, $1/2$, and $3/4$, complemented by "$1/f$" noise ($H_1 = 0$) and a regular function ($H_1 = 1$). All of these processes are have no intermittency ($C_1 = 0$) which increases vertically, as illustrated by the four multiplicative cascade fields at $C_1 = 0^+$, 0.05, 0.18, and 0.72. At the $(H_1, C_1) = (0,1)$ corner we find random Dirac δ-functions, at $(H_1, C_1) = (1,1)$, random Heaviside step-functions. Random devil's staircases (integrals of random multiplicative cascades) occupy the ($H_1 = 1, 0 < C_1 < 1$) border of the domain. A few stochastic models, documented in refs. [10,32], populate the interior of the domain where they can match the data. We have indicated the area where turbulent velocity lives (using quoted[39] values of the "intermittency parameter," $1-\tau(2)$, and a log-normal model[33–34] to go from $q = 2$ to $q = 1$) and, to facilitate comparison with turbulence, we have used $m = 2$ (the turbulence standard) in Eq. (4) for our LWC data , rather than $m = 1$ (as in the rest of this study).

- Ensemble-average (H_1,C_1)'s for internal cloud structure (according to LWC) do not[#] depend much on where the data was collected; there is no physical explanation for this universality yet.

- Detailed analysis of the FIRE database, 5 different cloud penetrations, shows variability in the (H_1,C_1)'s, i.e., non-ergodicity, primarily in the later (intermittency) exponent.

- As expected, column-integrated LWC = liquid water path (or LWP) is smoother $(H_1 \approx 0.37)$ than LWC $(H_1 \approx 0.29)$, and satellite imagery of reflected sunlight $(H_1 \approx 0.54)$ even more so.

- The intermittency of cloud structure, as measured by $C_1(\text{LWC}) \approx C_1(\text{LWP}) > C_1(\text{radiance})$, is considerably damped by the radiative transfer; numerical simulations have reproduced this.[38]

In summary, bi-fractal analysis can be used effectively in all types of data comparison studies, including model selection (by synthetic-to-real data comparison).

Table 1: *Bi-Fractal Properties of Cloud Data.* The SOCEX–1 program is described briefly in connection with Fig. 2; ASTEX (Atlantic Stratocumulus Transition EXperiment) took place in June-July 1992 in the Açores; it was "phase II" of FIRE (First ISCCP[†] Regional Experiment) which was started in 1987, off the coast of Southern California. All of the above were intense field programs focusing on marine boundary-layer clouds, with multiple research aircraft as well as ground-based instrumentation. In contrast, the ARM (Atmospheric Radiation Measurement) program is a U.S. Dep. of Energy initiative[1] designed as an on-going detailed study of the atmospheric column above a few selected sites within a GCM grid-box ($\approx$200 km on a side); the emphasis on the atmospheric radiation budget (therefore on the poorly understood role of clouds). Our LWP data was collected at the site in Oklahoma from microwave radiometry.

Database (dataset)	H_1	C_1	r_{min} / r_{max}	Reference No.
SOCEX–1 (07/26/93) LWC ensemble	0.31	0.11	5 m / 5 km	11
ASTEX'92 LWC ensemble	0.28	0.08	60 m / 60 km	8
FIRE'87 LWC ensemble	0.29	0.10	20 m / 20 km	10
FIRE LWC (6/30, 22:41Z)	0.29	0.14	20 m / 5 km	"
" " (7/02, 02:23Z)	0.22	0.15	" "	"
" " (7/14, 23:09Z)	0.34	0.03	5 m / 20 km	"
" " (7/16, 17:17Z)	0.31	0.08	20 m / 20 km	"
" " (7/16, 18:19Z)	0.34	0.07	" "	"
FIRE radiances (LANDSAT, 6/30)	0.54	0.06	150 m / 10 km	32
ARM LWP ensemble	0.37	0.08	1 min / 8 hr	40

3. STOCHASTIC MODELING OF CLOUDS, AND OTHER IMPORTANT CRITICAL PHENOMENA

There are at least three reasons to develop and study stochastic models. First, our cloud data analysis thrust is part of a larger agenda (cf. Fig. 1b) leading to cloud radiation studies using "realistic" cloud models, i.e., synthetic structures that reproduce those of real clouds. Second, we need the ability to generate artificial data with well-understood statistical properties in order to "feed" it, in controllable quantities, to data analysis computer codes; much like sophisticated laboratory or field instrumentation,[32] these analysis programs need to be tested and calibrated. Third, stochastic models are easily imported/exported from one discipline to another; being easier to understand than the physical systems, they indeed provide a forum where people in different areas of application can meet on a common ground.

[#]In contrast, scaling ranges and higher-order properties (cf. Fig. 4b) do vary with the regional climate.

[†]International Satellite Cloud Climatology Project.

3.1 "Bounded" Cascades: Simple to Build, Complex in Behavior

In our discussion of bi-fractal analysis, we commented on the current dearth of multifractal models for nonstationary processes. A simple prototype of a nonstationary multifractal model was developed[41] and used extensively in radiation studies[42] by one of the authors (RC) because its three parameters (spatial mean, log-variance, and spectral exponent β) can be tuned to reproduce LWP observations[43] of marine Sc under a broad range of conditions. However, potential applications of bounded cascades go far beyond stratiform clouds.

The generation procedure of a "bounded" cascade model is explained in Fig. 7, in relation to that of a parent-model used in the turbulence literature. That model is Meneveau and Sreenivasan's[20] primarily tutorial "p-model" (Fig. 7a); it is singular in the sense that the support of its PDF increases without bound with the number of cascade steps and it has stationary statistics ($\zeta(q) \equiv 0$) since $\beta = D_2 < 1$. In contrast, our nonstationary generalization (Fig. 7b) is absolutely bounded, hence $\tau(q) \equiv q-1$; it is nonetheless multifractal in the sense of Frisch and Paris[16] since[26]

$$\zeta(q) = \min\{qH,1\}, H \geq 0. \tag{13}$$

In particular, $1 < \beta = \min\{2H,1\}+1 \leq 2$ so we can match the large-scale behavior in Fig. 3.

There is a well-known formal analogy between multifractal exponents and relevant quantities of statistical thermodynamics which, in particular, justifies the terminology "partition function" used for $Z(q;r)$ in Eq. (5a-b): $q \leftrightarrow$ inverse temperature; $\tau(q) \leftrightarrow$ free energy; $1/r \leftrightarrow$ volume or number of particles (becomes very large in the "thermodynamic" limit); etc.[44] In the same spirit, a discontinuity in a derivative of a multifractal exponent function is interpreted as a phase transition. In the case of $\zeta(q)$ in Eq. (13), we are dealing with a 1st-order transition: at low temperature (high q), structure functions — closely related to the counterpart of partition functions $Z(q;r)$ for nonstationary signals[45] — are dominated by the rare but large jumps visible in Fig. 7b; at high temperature (low q), they are dominated by the frequent but small jumps, the "critical" temperature being $1/q_c = H > 0$.

The Legendre transform in Eq. (7) clarifies this picture. The large jumps are a manifestation of the stationary but highly non-Gaussian "phase" of the bounded cascade (viewed as a thermo-dynamical system): a Hölder exponent $h(x) = \zeta'(q) = 0$ ($q > q_c$), meaning a discontinuity in the signal, is found on a very sparse set of fractal dimension $D(h=0) = q\zeta'(q)-\zeta(q)+1 = 0-1+1 = 0$. The small jumps however are mapped to the Gaussian fBm-type but nonstationary "phase" of the system (with $\zeta(q) \propto q$): a Hölder exponent $h(x) = \zeta'(q) = H > 0$ ($q < q_c$) is found almost everywhere, i.e., on a space-filling set of dimension $D(h=H) = q\zeta'(q)-\zeta(q)+1 = qH-qH+1 = 1$. In essence, jumps occur only on lattice points and are substantial in magnitude when the system is cooled below $1/q_c = H$ while smaller jumps (steps) occur everywhere when the system is heated.

We find *finite* Lévy flights of index $\alpha \in (0,2)$ in the same universality classes defined by Eq. (13) for $H > 1/2$, with the correspondance[32] $H = 1/\alpha$; Lévy-stable processes also are often analyzed in terms of their "step" and "jump" components. It is noteworthy that financial time-series apparently have universal Lévy-type statistics (Alain Arnéodo, private communication). Is there a common feature between the complex geophysical system called "weather" that creates, deforms, and destroys clouds and the complex socio-technological system called "economy" that controls the market fluctuations? Or should we think of their similarities as purely coincidental? We are of the first opinion: both systems are energetically open and tend to operate at "criticality" in the sense of Per Bak.[46]
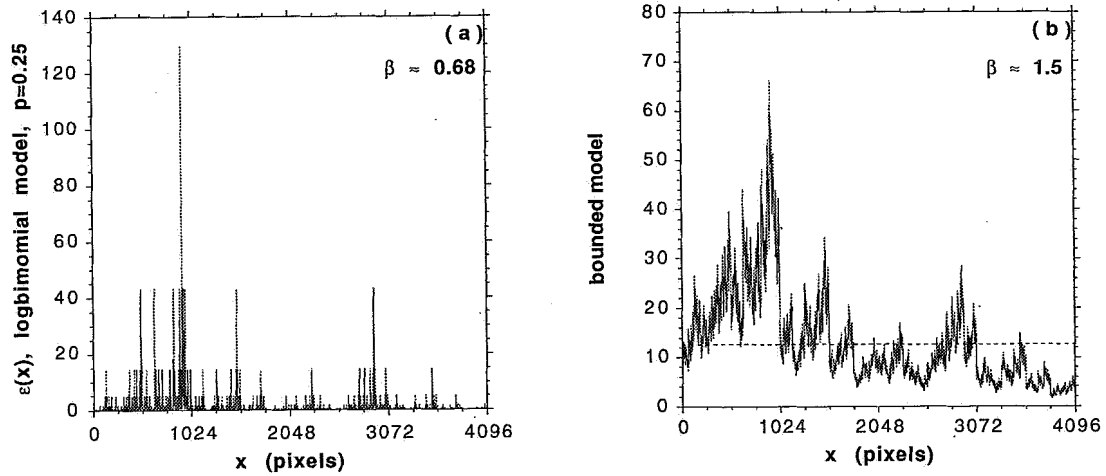
Figure 7: *Multifractal Cascade Models.* (a) Starting with a uniform measure on the unit interval, a singular "p-model" is generated by recursively dividing r-sized segments into two equal sub-segments and redistributing the measure in $[x,x+r]$ between the two halves; this amounts to multiplying the measure $\varepsilon(x)$ in each side by $W_\pm = 1\pm(1-2p)$, in this case, with $p = 0.25$. Meneveau and Sreenivasan,[20] the originators of this model (with the dissipation field of highly turbulent flows in mind), showed that, in Eq. (5b), we have $\tau(q) = -\log_2[p^q+(1-p)^q]$, $0 \le p \le 1/2$ (respectively, the "δ-function" and "uniform" limits). (b) A "bounded" cascade model generated exactly as described for the measure in panel (a) except that the multiplicative weights $W_\pm$ become closer to unity as the cascade proceeds to smaller scales: at the nth cascade step, the scale is $r_n = 1/2^n$ and $W_\pm(n) = 1\pm(1-2p)r_{n-1}^H$, with $H = 1/3$. A real-space renormalization argument[26] leads, in the limit $n \to \infty$, to $\tau(q) = q-1$ in Eq. (5b) and, in Eq. (2), $\zeta(q) = \min\{qH,1\}$ for $0 \le H \le \infty$ (respectively, the "singular" and "Heaviside-step" limits). Notice that the structure-function scaling is insensitive to p which controls the width of the lognormal-type 1-point PDF (see Fig. 11b). In summary, this "p,H-model" is essentially a nonstationary generalization of the p-model, with similar tutorial qualities.
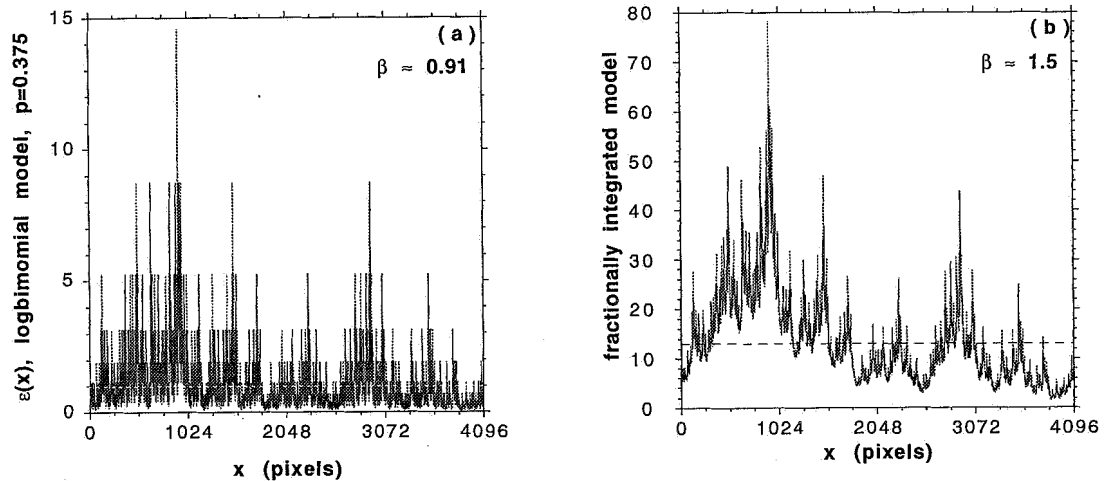

Figure 8: *More Cascade Models, Stationary and Not.* (a) As in Fig. 7a but with $p = 0.375$ (note the lesser variability). (b) The data $\varepsilon(x)$ in panel (a) has been low-pass filtered in Fourier space to yield $f(x)$, defined as the inverse FFT of $\tilde{f}(k) = \tilde{\varepsilon}(k)/|k|^{H^*}$, $H^* > 0$; the multifractal nonstationary behavior of $f(x)$ is described by Eq. (8) with $a = 1/H^*$ and $b = 1$, at least for low-enough order moments.[32,40] We have used $H^* = 0.29$, leading to the same $\zeta(2)$, hence β, as in Fig. 7b.
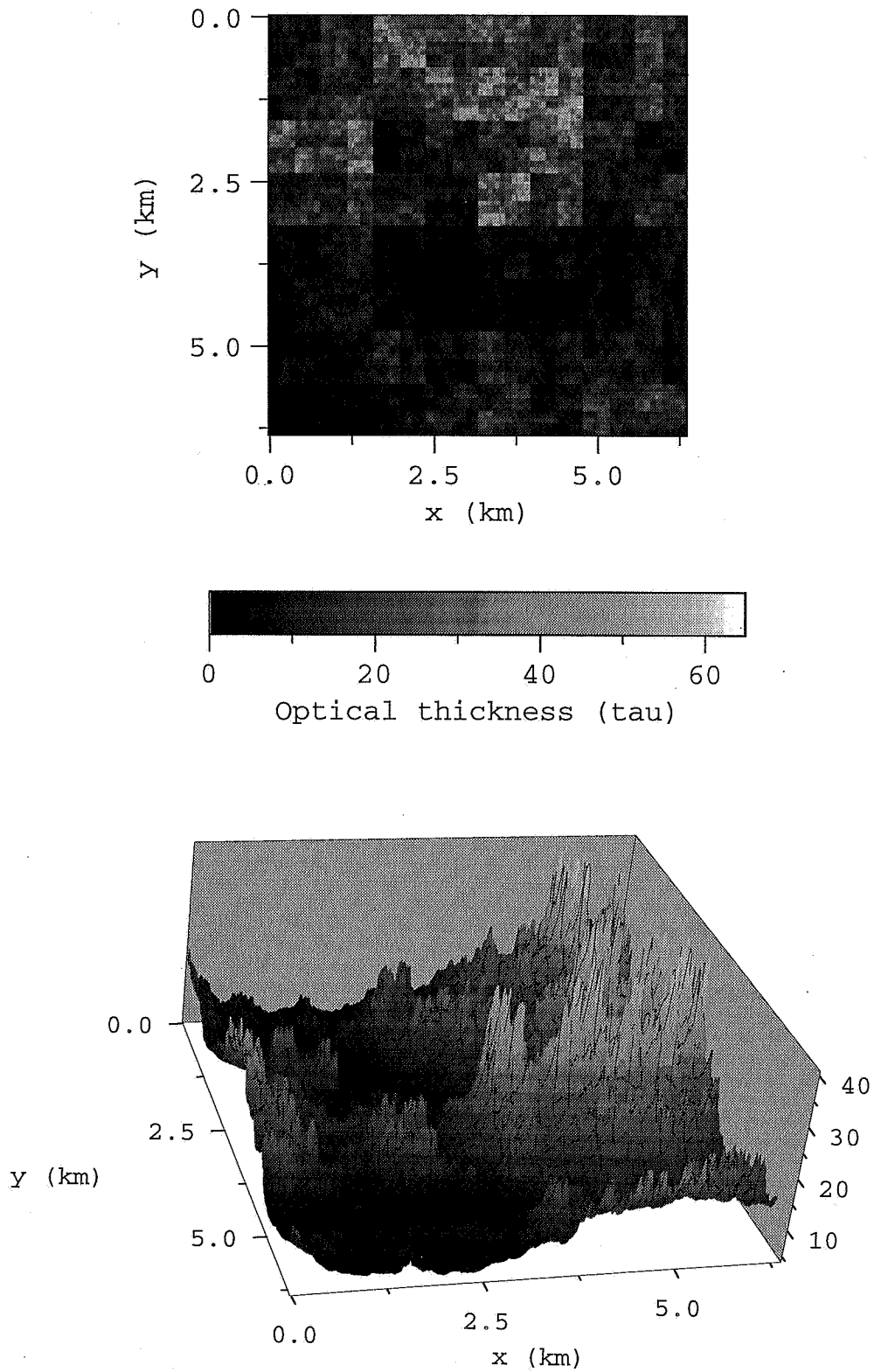
Figure 9: *Two-Dimensional Variability Models for Horizontally Extended Clouds.* (a) Gray-scale rendering of a bounded cascade model. (b) Perspective view of a fractionally-integrated model.

3.2 "Fractionally Integrated" Cascades: More Flexibility, Better Fit to Natural Signals

Bounded cascades are too simple to be "true" and, indeed, their tutorial quality comes at a cost: the rigidly prescribed structure-function scaling in Eq. (13). Furthermore, bounded cascades do not lend themselves gracefully to bi-fractal analysis. Indeed, we can dial any $H_1 = \min\{H,1\}$ from Eq. (11) but $C_1 = 0$ if $H < 1$, and $C_1 = 1$ otherwise in Eq. (12b) with $b = 1$, for simplicity. This is not helpful for cloud modeling in a "post-spectral analysis" framework.

A stochastic model with continuously variable intermittency was proposed by Schertzer and Lovejoy[35] for rain and clouds, landscape or any other compliant multifractal geophysical field.[92] Given a singular multiplicative cascade (with a certain C_1 between 0 and d, the dimensionality of space), we can "tune" the spectral scaling to any prescribed value simply by power-law filtering in Fourier space. So, if we want an end-product $f(x)$ in $d = 1$ that obeys Eq. (1) with $\beta > 1$ and we have an input field $\varepsilon(x)$ that has $\beta_\varepsilon = \tau(2)$, the desired filter must scale in k^{-H^*} where the exponent $H^* = (\beta - \beta_\varepsilon)/2$. Figure 8 shows an example based on a singular cascade using a Meneveau-Sreenivasan p–model:[20]

$$\tau(q) = -\log_2[p^q + (1-p)^q].\tag{14}$$

Equations (10a–b) with $a = 1/H^*$ and $b = 1$ describe the fractionally-integrated cascade model;[35] a little algebra leads to

$$H_1(p,\beta) = H^* = \frac{1}{2}\big(\beta + \log_2[1 - 2p(1-p)]\big),\tag{15a}$$

as long as it is < 1. The input field $\varepsilon(x)$ is responsible for the intermittency in the final output; for the p-model it is parameterized by

$$C_1(p) = 1 + p\log_2 p + (1-p)\log_2(1-p).\tag{15b}$$

The choice of model for the singular cascade is quite arbitrary. A p-model is exactly log-binomial for a finite number of cascade steps; more variability can be obtained with a log-normal model:[35,39]

$$\tau(q) = (1 - C_1 q)(q - 1),\tag{16}$$

conveniently parameterized directly in terms of C_1. For $q = 2$, we find $\beta_\varepsilon = \tau(2) = 1 - 2C_1$; again using Eq. (10b) with $b = 1$ and $a = 1/H^*$, this leads to $H_1(C_1,\beta) = H^* = H_2(\beta) + C_1 = (\beta - 1)/2 + C_1$.

3.3 Cloud Models with 2D Horizontal Variability

It is straightforward to generalize the 1D procedures described in the last sections in 2D space. Starting with bounded cascade models, we only need to properly parameterize the singular cascade in two spatial dimensions. The 1D p-model in Fig. 7a has a single parameter; its most general 2D counterpart has three.[32] The unit square is evenly "loaded" then divided into 4 equal sub-squares; let $0 \leq p_i \leq 1/2$ ("i" = "x", "y", "d") stand for the ratios we use to transfer randomly "mass" between E and W (parallel to x-axis), N and S (parallel to y-axis), and from NE/SW to NW/SE (from one diagonal to the other). Equivalently, the uniform measure $\varepsilon(x,y)$ on $[0,1)^2$, is multiplied successively by $W_i = 1 \pm (1 - 2p_i)$ in the 4 sub-squares, and so on, at smaller scales. If a rough multifractal surface instead of a singular measure is desired, use $W_i = 1 \pm (1 - 2p_i)/(2^{n-1})^H$ where $n \geq 1$ is the order of the cascade step.

Figure 9a shows a 2D bounded cascade on a gray scale for $n_{max} = 7$, with $H = 1/3$ and the p_i's drawn randomly from $\{0.45, 0.43, 0.41\}$. The obvious shortcoming of this model is its x,y-grid anisotropy, traceable to the discrete nature of the cascade. One way of constructing a grid-free model is to use "scale-wise continuous" cascades. A scale-wise continuous singular cascade with stationary lognormal statistics is obtained by exponentiating Gaussian $1/f$ noise (white-noise filtered in $k^{-1/2}$).[35] Exponentials of more powerfully filtered Gaussian white-noise will clearly lead to lognormal models with nonstationary statistics.* Alternatively, one can apply a power-law filter to a singular cascade in 2D Fourier-space;[35,48] Fig. 9b shows a perspective view of such a 2D fractionally-integrated continuous log-normal cascade.

4. CLOUD-RADIATION INTERACTION – 1: ILLUMINATION BY SOLAR BEAM

We have already stated in §1.2 that there are three standard objections to fractal cloud modeling emanating from mainstream meteorology: no fluid dynamics, no thermodynamics, and no optics. In this section, we describe the most salient results obtained in the course of removing the last objection by applying radiative transfer theory to cloud models based on one or another of the synthetic random fields described in the previous section and Figs. 7–9.

4.1 General Considerations

Transport of solar photons through vertically stratified but horizontally homogeneous model atmospheres — including cloud layers — is well-understood. This "plane-parallel" theory is liberally applied by meteorologists in both climate and remote-sensing studies: either exact[49] or approximate[50] approaches are used depending on the amount of computer time allocated to the task. Here, we distinguish between "exact" and "approximate" methods only by the degree of angular detail in the description of the radiance field. Operational procedures invariably use some computationally fast approximate transport theory, or else vast look-up tables generated by using an exact method for once and for all.

There are also two fundamental options for radiative transfer in horizontally variable media :

- invoke an independent pixel (IP) approximation which amounts to using (exact or approximate) plane-parallel theory locally, at the cost of neglecting horizontal radiative fluxes;
- allow horizontal fluxes by using an (exact[51–52] or approximate[53–54]) theory, our preference being Monte Carlo (MC) simulation for its simplicity in implementation — an exact approach.

Figure 10 describes schematically the IP approximation and the principle of an exact MC solution for a generic optical medium with a horizontally variable photon mean free path (MFP). MFP is the inverse of "extinction" σ, the probability of photon/droplet interaction per unit length along the beam; σ is determined mainly by the density of cloud droplets, hence LWC (*in situ* measurements discussed in section 2).

Other key ingredients in radiative transfer theory are:

- $\varpi_0 = \sigma_s/\sigma \leq 1$, the ratio of cross-section for scattering only over total cross-section; and
- $d\sigma_s/d\Omega$, the differential cross-section for scattering from which we define the asymmetry factor,

---

*Non-scaling filters have also been used to obtain stationary (e.g., $\beta = 0$) and nonstationary (e.g., $\beta = 5/3$) regimes in the same model on either side of a prescribed integral scale.[47]
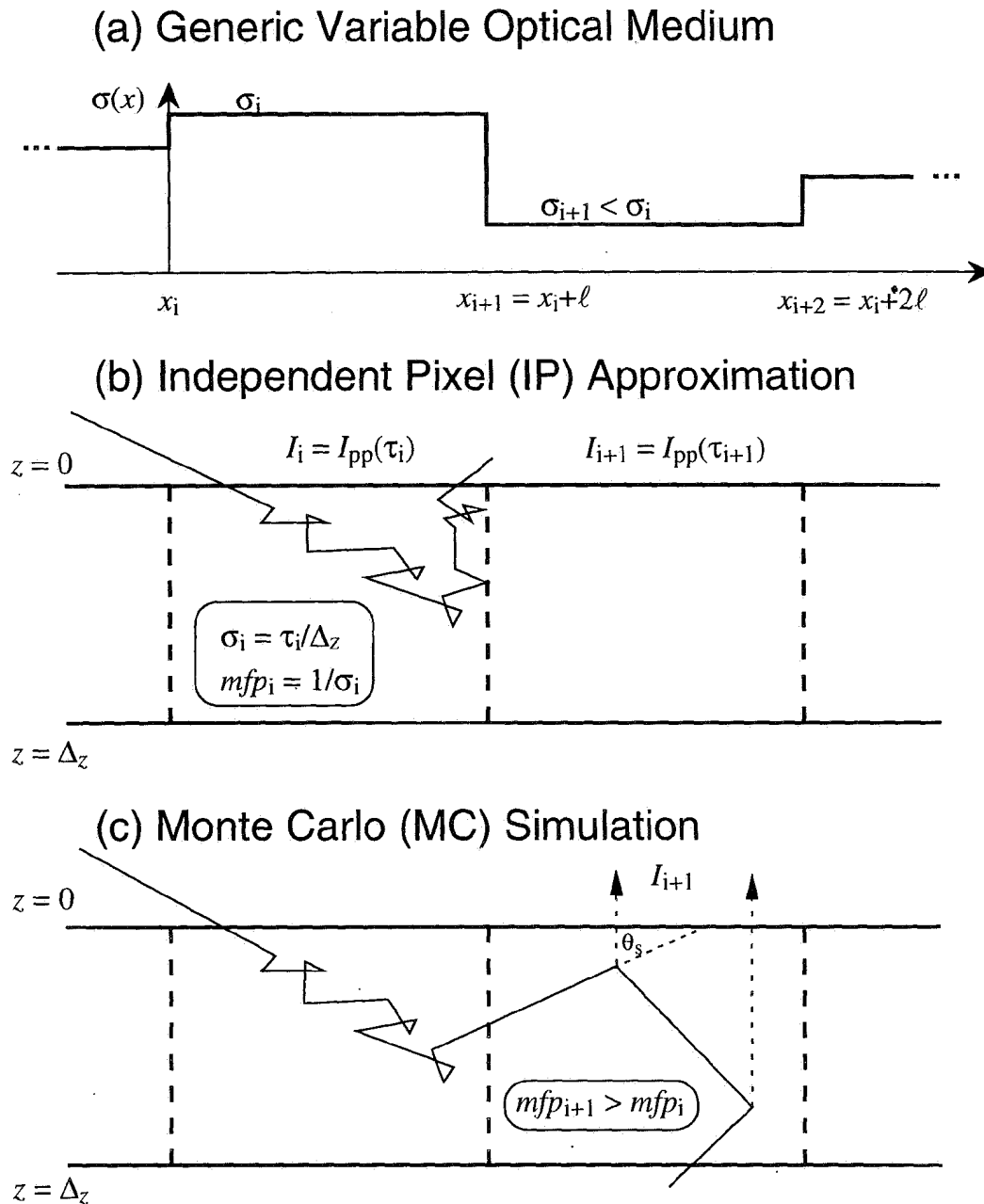
(a) Generic Variable Optical Medium

$\sigma(x)$ σ_i

$\sigma_{i+1} < \sigma_i$

x_i $x_{i+1} = x_i + \ell$ $x_{i+2} = x_i + 2\ell$

(b) Independent Pixel (IP) Approximation

$z = 0$

$I_i = I_{pp}(\tau_i)$ $I_{i+1} = I_{pp}(\tau_{i+1})$

$\sigma_i = \tau_i / \Delta_z$

$mfp_i = 1/\sigma_i$

$z = \Delta_z$

(c) Monte Carlo (MC) Simulation

$z = 0$

I_{i+1}

θ_s

$mfp_{i+1} > mfp_i$

$z = \Delta_z$

Figure 10: *Radiative Transfer in Heterogeneous Media with Uniform (Sun-like) Illumination.* (a) Portion of a spatially variable extinction field: a denser pixel, followed by a more tenuous one. (b) A simplified approach: each pixel behaves like a homogeneous plane-parallel optical medium with the same properties as assigned to the pixel by the variability model; this amounts to making the pixel's boundaries reflective (or cyclical). In this "Independent Pixel" (IP) approximation, radiative responses for larger-than-pixel scales are obtained by straightforward spatial averaging. (c) An exact solution: Monte Carlo (MC) simulation. In this technique, many realizations of "photon" random walks are generated, from impact to escape, using the appropriate rules of propagation and scattering. At each scattering, a weighted contribution to the local estimate of radiance viewed from a distant observer is computed. At each escape, the local value of flux is incremented by the weight of the photon. The photons weight is deceased at each scattering, to account for the possibility of absorption. Radiative responses in flux or radiance, at any desired scale, are obtained by averaging over the random walks , the scatterings, and space.

$$g = \frac{1}{\sigma_s} \int \Omega{\bullet}\Omega' \, d\sigma_s(\Omega{\bullet}\Omega'),$$ (17)

where Ω and Ω' denote respectively the incident and outgoing directions, so $\cos^{-1}(\Omega{\bullet}\Omega')$ is the scattering angle.

They both depend on the real and imaginary parts of the refraction index of water (plus eventual impurities) at the wavelength of interest, and on the precise size-distribution of the cloud droplets. For typical droplet populations,[90] we have $\varpi_0 = 1$ (pure scattering) at visible wavelengths, somewhat less ($\varpi_0 \approx 0.98$) in the near-IR, and $g \approx 0.85$. The main utility of the asymmetry factor is to define the so-called "transport" MFP[55]

$$l_t = \frac{1}{(1-\varpi_0 g)\sigma}$$ (18)

which accounts parameterically for the forward scattering in Eq. (17). After $\approx(1-g)^{-1}$ scattering events (assuming $\varpi_0 = 1$) that are generally in the forward ($\Omega{\bullet}\Omega' > 0$) direction, photons lose track of their original bearing; in the meantime, they cover (on average) that much more distance in the original ballistic direction.[56] For all practical purposes, l_t is the MFP for one "effective" isotropic ($g = 0$) scattering.

Figure 11a shows the important radiative responses — reflectance (or "albedo"), transmittance, and absorptance — of homogeneous plane-parallel anisotropically ($g = 0.85$) scattering media, with and without absorption, as a function of their "optical" depth:[*]

$$\tau = \sigma \Delta_z$$ (19)

which is the dimensionless ratio of physical cloud thickness Δ_z to photon MFP, $1/\sigma$. It can be shown that $\tau \propto$ LWP, measurements of which were described in section 2. Asymptotic (large τ) radiative transfer theory[91] is accurate enough for most cloud studies and was used in Fig. 11a; its natural independent variable is "rescaled" optical depth

$$(1-\varpi_0 g)\tau = \Delta_z/l_t,$$ (20)

which can be interpreted as effective optical depth for isotropic scattering. Any object considered "opaque," most clouds in particular, will have $(1-\varpi_0 g)\tau \geq 1$.

Table 2: Physical and Optical Properties for Marine Stratocumulus Clouds.

Name	Symbol	Typical Value and/or Range	Unit
Optical Depth:	τ	13, 4 – 60	-
Geometrical Thickness:	Δ_z	0.2 – 0.4	km
Asymmetry Factor:	g	0.85	-
Single-Scattering Albedo:	ϖ_0	1.00 (visible) 0.98 (near-IR)	-
Extinction:	$\sigma = \tau/\Delta_z$	40, 10 – 180	1/km
Photon Mean-Free-Path:	$l = 1/\sigma = \Delta_z/\tau$	20, 3 – 100	m
Transport Mean-Free-Path:	$l_t = l/(1-\varpi_0 g)$	150, 20 – 600	m
Rescaled Optical Depth:	$\Delta_z/l_t = (1-\varpi_0 g)\tau$	2, 0.6 – 9	-

[*] Notation choice in Eq. (19)/Fig. 11a is traditional and confusion with the exponents in Eq. (5b)/Fig. 5b is unlikely.
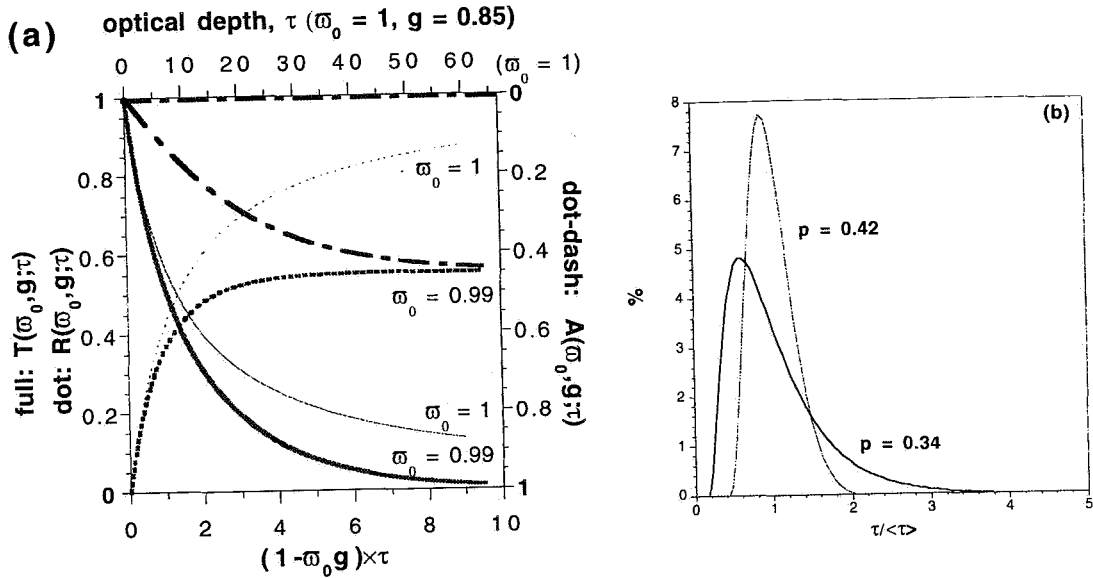
Figure 11: *Input for the Computation of Large-Scale Radiative Properties of Heterogeneous Cloud Models in the Independent Pixel (IP) Approximation.* (a) Radiative properties of homogeneous scattering/absorbing plane-parallel optical media in the diffusion limit. These are the highly idealized cloud models and the solar radiative transfer theory used in the energetics of GCMs as applied, for instance, to climate forecasting. (b) Quasi-lognormal PDFs of bounded cascades used to model the variability of optical depth, the abscissa in panel (a).
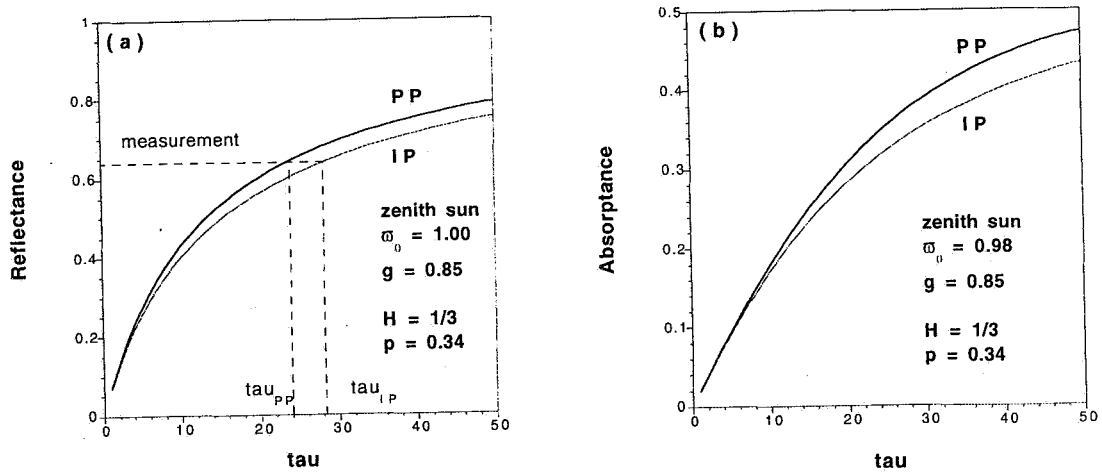

Figure 12: *Radiative Properties of Opaque Heterogeneous Plane-Parallel Media in the IP Approximation.* Geometrical thickness is constant but optical thickness varies horizontally according to a bounded cascade model; parameters are set to reproduce the observed structure of marine stratocumulus clouds. (a) Reflectance in the purely scattering case, for homogeneous and fractal models. (b) Same as panel (a) but for bulk absorptance when scattering-to-absorption probability ratio is 98÷2.

In contrast to the highly variable τ, ranging from less than 5 to over 50, marine Sc have relatively constant Δ_z, in the range 0.2–0.4 km. Upper-boundaries of marine Sc are especially well-defined (flat) due to their occurrence just under a strong inversion in the stratified temperature field, stabilized by radiative cooling by thermal emission. Important Sc properties are summarized in Table 2.

4.2 Large Scales: The Albedo Problem and the Cloud Absorption Anomaly

Any large-scale cloud radiative property is easily computed within the IP approximation by averaging the appropriate function in Fig. 11a with the PDF of optical depth relevant to the cloud variability model. Figure 11b shows PDFs of $\tau/\langle\tau\rangle$ for bounded cascade models with the same $H = 1/3$ and different p-values compatible with observations;[57] optical depth is obtained by multiplying the random variable by the prescribed mean $\langle\tau\rangle$.

Figure 12a shows, as a function of $\langle\tau\rangle$, the systematic bias in the domain/ensemble-average albedo when variability is totally ignored (upper curve) in comparison with IP predictions for cloud models based on a bounded cascade (lower curve) at wavelengths (e.g., ≈ 0.5 μm) where cloud droplets are purely scattering (the imaginary part of liquid water's refractive index vanishes).[42] The reason for the bias is clear: reflectance is a concave function $R(\cdot)$ of the random variable τ (its graph is above any two points on the graph), so $\langle R(\tau)\rangle < R(\langle\tau\rangle)$ (by Jensen's inequality). Implications of the bias in albedo are tremendous. In GCM-based climate studies, the dynamics predict LWP, hence $\langle\tau\rangle$, for a given grid-point (≈ 200 km wide); without substantial "tuning" of $\langle\tau\rangle$, the corresponding albedo will be too large.[58] In atmospheric remote sensing, we wish to determine LWP, via $\langle\tau\rangle$, at the smallest observable scale. However, most operational satellites do not see details below tens of kilometers, so there is plenty of unresolved variability; Fig. 12a also shows that satellite radiances lead to substantially underestimated local optical depth values.[59]

Figure 12b is the counterpart of Fig. 12a for bulk absorptance of solar radiation by the cloud; this critical non-dimensional quantity is used in dynamical models to compute the amount of energy deposited in the cloudy layer of the atmosphere. (In terms of wavelength, we can think of the near-IR or a "broad-band" integration over the solar spectrum.) Figure 12b shows that, within the IP approximation, variability reduces absorptance for the same reason it reduces reflectance: it is concave with respect to τ. Far from explaining a documented observational problem as was the case for reflectance, the prediction for absorption contradicts recent analyses of surface-satellite[60-61] and two-aircraft[62-63] observations that uncovered a substantial enhancement of absorptance with respect to plane-parallel model computations. This is still a controversial result.[64-66] Since the alleged discrepancy seems to increase with cloudiness, it is known as the "cloud absorption anomaly." The approximate nature of IP computations is not the issue here, nor is the identification of "interstitial" absorption by gases with absorption by the scattering particles (i.e., droplets). Indeed, detailed MC simulations, at best, compensate for the absorptance deficit between homogeneous and IP results.[67] Other case-studies[68-69] have shown that only a portion of the anomaly can be explained by 3D radiative transfer effects, namely, increased photon paths.

4.3 Small Scales – 1: Radiative Smoothing and the LANDSAT Scale-Break

Returning to purely scattering wavelengths, we address the important issue of validation of the attractive IP approximation for clouds. At what scale do horizontal fluxes become important? How can we measure "importance"? What mechanisms determine the magnitude and sign of horizontal fluxes? Are there other parameters than scale we need to consider?

These questions are far from having final answers at present. However, considerable progress has been made at non-absorbing wavelengths for boundary-layer clouds (such as marine Sc) that are horizontally extended (hence geometrically plane-parallel) with plenty of internal variability. From the outset, the above questions can only be addressed in the framework of 2-point (or more sophisticated) statistics of all orders; the 1-point means over the whole computational domain used in §4.2 are not enough. Also we need to define the inner- and outer scales of the cloud model: respectively, ℓ and L, hence the total number of pixels $N_{tot} = (L/\ell)^d$ for $d = 1,2$.

Figure 13 shows how radiative transfer "smoothes" the fractal fluctuations of the underlying cloud structure.[38] Panels (a–b) show how the large-scale albedo field — *apparent* cloud structure (according to a remote observer) — closely follows the fluctuations of the optical depth field — *inherent* cloud structure (according to an internal observer). In panel (c), the wavenumber spectra of the IP and MC fields are indistinguishable in this regime; furthermore, they are both in sync with that of the non-differentiable $\tau(x)$ field, with prescribed $\beta \approx 5/3$ scaling. This is no longer true for scales less than the (reflective) radiative smoothing scale η_R, which is ≈ 0.5 km (≈ 40 pixels) here; at these small but resolvable scales, the MC albedo field looks like a local average of the IP field. Accordingly, the MC field's spectrum in panel (c) decays fast enough to talk about differentiability ($\beta \geq 3$), numerical noise notwithstanding. Panel (d) shows the run of qth-order structure function exponents $\zeta(q)$ versus q for the various fields:

- Considering the diminutive scaling range of the small-scale regime, deviation from the straight line $\zeta(q) = \zeta'(0)q \approx q$ for the MC field, is likely to fail the multifractality test outlined in §2.4.
- In sharp contrast with small q's (less than ≈ 3), high-q scaling is different for IP (or MC) and the given multifractal $\tau(x)$ field at large scales, meaning that large-and-rare jumps in optical depth are more smoothed than their small-but-frequent counterparts — enough to change the scaling rather than simply reduce the scaling range.[*]

In our task of defining the domain of validity of the IP approximation, this last finding is a natural complement in q-space (hence event-space) to the r-space (scaling-range) reduction. To the best of our knowledge, this is the first application of multifractal statistics to a practical problem in atmospheric radiation: quantitative assessment of the verisimilitude of apparent (hence remotely-sensed) cloud structure with respect to the inherent (and, generally speaking, unknown) structure.

Extensive numerical experimentation showed that, almost independently of all other parameters (including choice of scale-invariant cloud model in Fig. 8, at a given β), we have[72]

$$\eta_R \sim \frac{\Delta_z}{\sqrt{(1-g)\langle\tau\rangle}},$$ (21)

with a proportionality constant in the range 2–3. Wavenumber spectra of radiance fields for very overcast situations, observed by satellites at visible (0.5–0.7 μm) wavelengths, show strong evidence of radiative smoothing.[43,72–73] Indeed, LANDSAT cloud scenes (many of marine Sc during FIRE) have high enough resolution (80-m and 30-m) to resolve the scale-break at η_R in Fig. 13c. The typical marine Sc parameters in Table 2 yield 0.2–0.3 km for the r.h.s. of Eq. (21).

---

[*]In a preliminary account of radiative smoothing,[71] the unfortunate use of a 2D cloud model with a limited range of scales and inevitably noisy numerics lead to the erroneous conclusion that it changes even the spectral ($q = 2$) scaling.
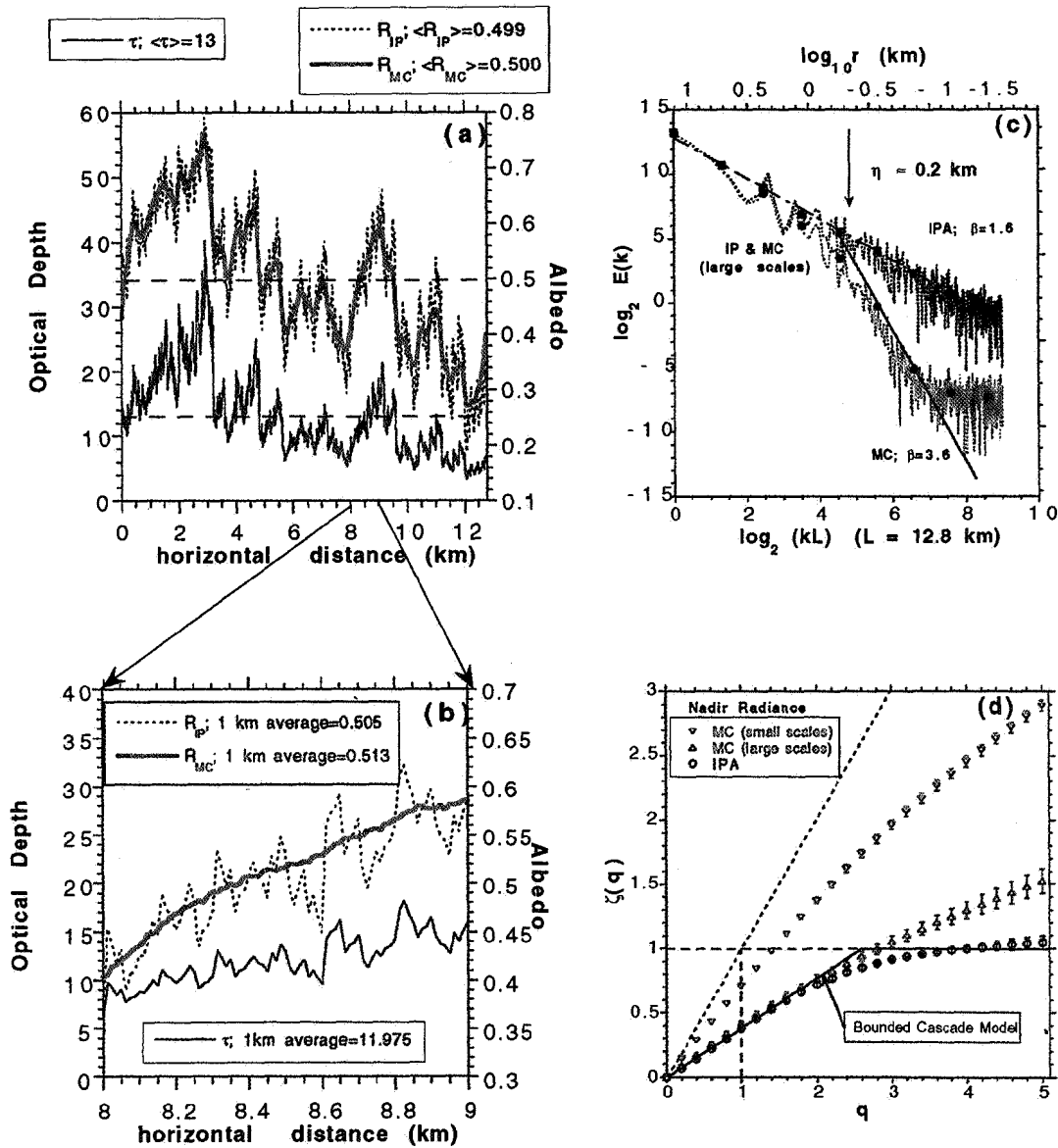
Figure 13: *Radiative Smoothing in Fractal Sc Cloud Models.* (a) IP and MC reflectance fields for a 1D cloud model (also illustrated) derived from Fig. 7b with mean optical depth $\langle\tau\rangle = 13$ for solar zenith-angle 22.5°. Other parameters are: physical thickness $\Delta_z = 0.3$ km; $\varpi_0 = 1$ (pure scattering); and a Henyey–Greenstein[70] scattering kernel, entirely defined by $g = 0.85$ in Eq. (17), was used. The entire computational domain ($L = 12.8$ km) is illustrated, the pixel-scale being $\ell = 12.5$ m. (b) "Zoom" into a 1 km section of the fields in panel (a). (c) Wavenumber spectra of the IP (scaling) and MC (non-scaling) fields in panels (a–b), combined with those of another realization of the (10-step) bounded cascade model to reduce the statistical noise-level; the fundamental "radiative smoothing" scale $\eta_R \approx 0.2$ km is highlighted and we notice the uncorrelated (white) MC noise at the smallest scales. (d) Multifractal exponents $\zeta(q)$ for nadir-viewing radiance fields in the large-scale (IP & MC) and small-scale (MC only) regimes; for lack of data, the deviation of the small-scale exponents from $\zeta(q) = q$, corresponding to everywhere continuous and almost everywhere differentiable fields, is probably spurious in the sense of §2.4.
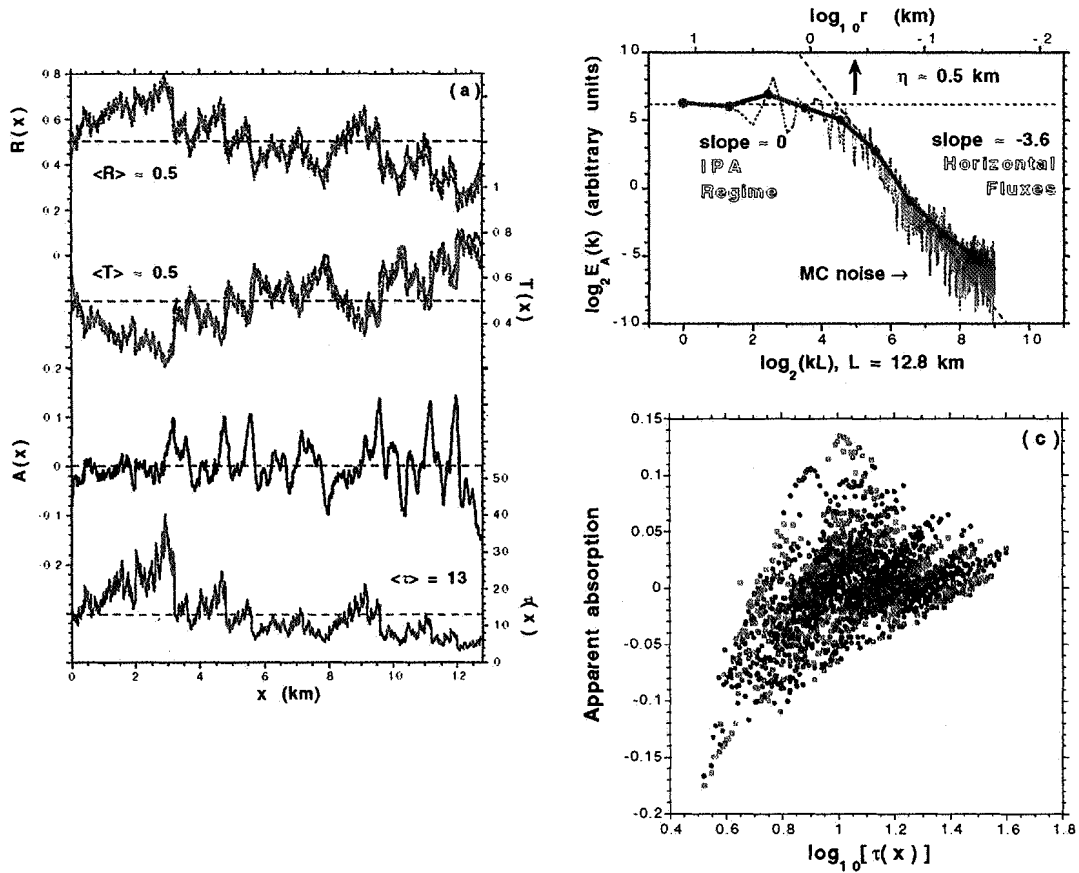
Figure 14: *Apparent Absorption in a Purely Scattering 1D Cloud Model and Radiative "Channeling."* (a) From top down, local albedo $R(x)$ and transmittance $T(x)$ for IP and MC, $A(x)$ in Eq. (22), and $\tau(x)$ vs. x; the first and last fields are reproduced from Fig. 13a. (b) Wavenumber spectrum of the data in panel (a), combined with that of another realization of the cloud model. (c) Scatter-plot of $A(x)$ versus $\log_{10}\tau(x)$ for two other numerical simulations (resp. red and black symbols), similar to panel (a) but with over-head sun rather than 22.5° off-zenith; note how the horizontal flux field tends to converge, meaning $A < 0$, (or diverge, $A > 0$) for low (high) cloud optical depth.

4.4 Small Scales – 2: Apparent Absorption and Radiative Channeling Processes

Radiative smoothing has important consequences for the empirical determination of the radiative energy budget of a cloud-laden atmospheric column, including the absorption within it.[47,74] A typical radiative budget computation involves a *net* radiative flux at the top of the column (either cloud top or higher) and at the bottom of the column (between cloud base and surface). Net fluxes are differences between down- and up-welling fluxes at a point, or averaged over a finite area. In Figs. 13a–b, we have plotted local albedo $R(x)$, $0 \leq x < L = 12.8$ km (on a grid of constant $\ell = 12.5$ m), defined as the up-welling flux at cloud top; down-welling flux is the unitary illumination, so net flux is $1–R(x)$. Similarly, net flux at cloud base is $T(x)–0$, i.e., transmittance down, nothing up (we are assuming a purely absorbing surface, well approximated by ocean). *Apparent* absorption in the cloud is the difference in net fluxes

$$A(x) = [1–R(x)]–[\ T(x)–0] = 1–[R(x)+T(x)]. \tag{22}$$

Figure 14a shows $A(x)$, and its two components, for the MC simulation in the same purely scattering 1D fractal cloud as used in Fig. 13a. The IP prediction for this field is $A(x) \equiv 0$ but radiant energy conservation only requires the domain average of its MC counterpart to vanish and, sure enough, broad fluctuations develop on smaller scales. The order-of-magnitude of the net horizontal fluxes inside the cloud can be estimated from that of $|A(x)|$; not surprisingly, it is commensurate with the discrepancy in the cloud absorption anomaly issue.[75] In other words, the anomalous part of the *true* absorption "signal," if it exists, is essentially buried a "noise" of *apparent* absorption coming from natural variability. This underscores the difficulty of true absorption measurements and, from there, the importance of using adequate spatial sampling and averaging strategies.[74]

Figure 14b shows the wavenumber spectrum of $A(x)$ in Fig. 14a, along with another realization. Viewed as a stochastic process, we see two regimes: a small-scale (large k) nonstationary, even smooth, regime characterized by scaling in $\beta > 3$; and a large-scale (small k) stationary regime of uncorrelated fluctuations, similar to white ($\beta = 0$) noise. Transition occurs at the integral scale which we can identify with the relevant smoothing scale:[75] $\eta = \max\{\eta_R,\eta_T\}$ where $\eta_T \sim \Delta_z$ (cf. §5.3 below). In these two regimes, the dominant radiation transport modes are respectively "IP" (no horizontal fluxes) and "MC" (significant horizontal fluxes) for large and small scales; *true* absorption can only be estimated in the former.

Finally, synthetic $\tau(x)$ and $A(x)$ data is to illustrate the mechanism that determines the sign of horizontal fluxes: in Fig. 14c, we see that $A(x)$ correlates with $\log\tau(x)$. The physical meaning of this trend in apparent absorption is that solar photons — viewed collectively as fluid in a pressure-driven flow through a porous substrate — are repelled by dense regions (look like photon sinks from outside, $A(x) > 0$), and they are funneled into tenuous ones (look like sources, $A(x) < 0$).[76] This intrinsically higher-dimensional process, known as "radiative channeling" in the astrophysical literature,[77] is responsible for the smoothing observed in our simulations for fractal stratocumulus and in the corresponding LANDSAT imagery. However, channeling certainly occurs in more singular situations, such as broken cloud systems, as well.[78–80]

5. CLOUD-RADIATION INTERACTION – 2: ILLUMINATION BY LASER BEAM

It is realized here that problems of uniform illumination of realistic heterogeneous clouds can be clarified by localized illumination of idealized homogeneous clouds, and this leads to new instrument design.

5.1 Green-Function Analysis of Radiative Smoothing

As a summary of many numerical experiments, Eq. (21) begs for a physical explanation. As the primary control mechanism of horizontal fluxes in variable optical media, radiative channeling is relevant to radiative smoothing but is also too generic. Clearly, the smoothing scale η_R in Eq. (21) describes the extent of horizontal photon transport in the fractal cloud. The part of the horizontal transport due to net horizontal fluxes excited by the variability — channeling *oblige* — is necessarily *anisotropic* in space. There is also an *isotropic* component in horizontal photon transport simply due to the random nature of their propagation in the cloud, from impact to escape. This aspect of radiative smoothing can be investigated with homogeneous clouds under non-uniform illumination. In the case of a Dirac δ-illumination, the resulting field is the cloud's radiative Green function.

Figure 15a shows the reflected radiation field for collimated point-wise illumination of an idealized homogeneous cloud of optical depth $\tau = 13$ and thickness $\Delta_z = 0.3$ km; Fig. 15b shows the counterpart for (the central portion of) a fractal cloud the same thickness (held constant) and $\langle \tau \rangle = 13$. The more or less equidistant isophotes on a log-scale are characteristic of an exponential decay. A convenient measure of horizontal photon transport prior to reflection, with or without perturbation by fractal variability, is the root-mean-square (r.m.s.) displacement, equivalently, the 2nd-order central moment of the fields in Figs. 15a–b, denoted $\sqrt{\langle \rho^2 \rangle_R}$.

Figure 16a shows $\langle \rho^2 \rangle^{1/2}$ in units described by the r.h.s. of Eq. (21) as a function of $(1-g)\tau$ for homogeneous clouds and $(1-g)\langle \tau \rangle = \Delta_z \langle l_t^{-1} \rangle$ for fractal clouds, considering Eqs. (18–19). Results in Fig. 16a can be summarized simply as

$$\langle \rho^2 \rangle_R^{1/2} \approx \sqrt{\Delta_z l_t},\tag{23}$$

and we see that fractality boosts $\langle \rho^2 \rangle_R^{1/2}$ by a modest change in the prefactor. Since the r.h.s.'s of Eqs. (23) and (21) are identical, the LANDSAT scale-break is largely explained by horizontal photon transport.*

The predictions in Figs. 15b and 16a have received direct confirmation by observation of real clouds: the laser beam of a conventional ground-based atmospheric lidar system was deflected from zenith, leaving the detector (in pulse integration mode) pointing to zenith. Figure 15c shows numerics and measurements for radiance versus zenith angle: the exponential far-field is readily resolved, natural variability and limited instrumental sensitivity notwithstanding.[81]

A noteworthy application of the Green functions in Figs. 15a–b is a computationally efficient alternative to MC simulation that yields very realistic radiance fields. Starting with radiances obtained within the IP approximation, we smooth this field (via direct and inverse FFTs) by convolution with the relevant Green function. We call this the "Nonlocal IP Approximation," or NIPA.[38] Conversely, an observed radiance field can be "roughened" prior to extraction of optical depths in order to obtain more realistic values than with the standard IP approximation. We call this the inverse NIPA.[82] Considerable caution is required in this last procedure because the associated de-convolution operation is numerically unstable (an "ill-posed" problem), in the sense that small differences are amplified; this problem is solved by standard[93] regularization techniques.

---

*The numerical result in Eq. (19) and the analytical theory described in section 5 ruled out a number of other physical[43] or statistical[73] explanations of the "LANDSAT scale-break" advanced in the literature.
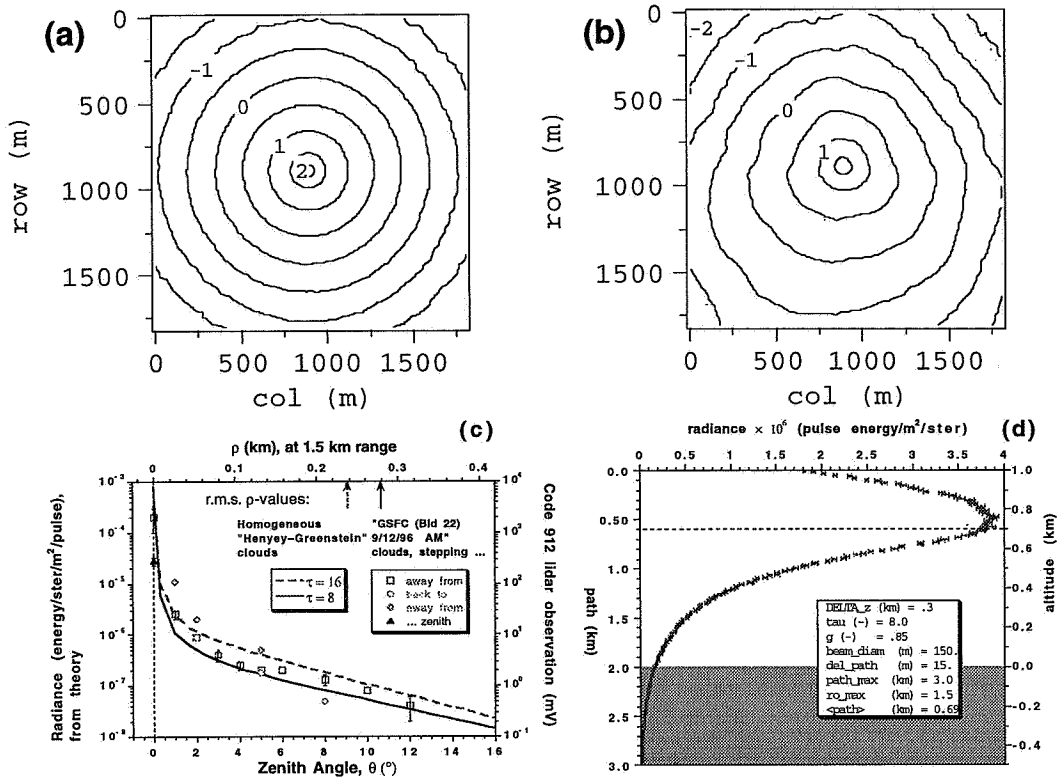
Figure 15: *Remotely Observable Parts of Radiative Green Functions.* (a) Isophotes for localized and collimated but steady illumination of a homogeneous plane-parallel cloud with $\tau = 13$ and $\Delta_z = 0.3$ km. (b) Same as in (a) but for a fractal cloud same (constant) thickness and optical depth (in the mean). (c) The two curves are path-integrated angular Green functions for homogeneous clouds with $\tau = 8,16$ and $\Delta_z = 0.3$ km observed from a close range (1.5 km = $5 \times \Delta_z$) as would be the case for a wide-angle imaging lidar (WAIL) system at ground level. The symbols, referring to the r.h. axis, are observations of real clouds; though uncalibrated and subject to natural variability, they clearly show the characteristic exponential decay of the diffusive far-field. (d) Temporal Green function for a homogeneous cloud with $\tau = 8$ irradiated with a laser pulse then spatially integrating over most of the "spot" in panel (a); time has been converted to total photon path λ (l.h. axis, increasing downward). In the conventional lidar theory, "range" = $\lambda/2$ is used to position the origin of the "echo;" the r.h. axis is range converted into altitude above sea-level, as seen from a space-borne lidar system, for a typical marine Sc layer. Notice the echoes originating apparently from below the surface —such observations were made during the LITE mission.
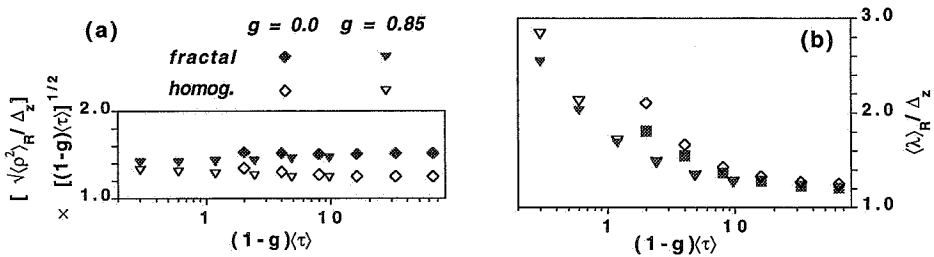

Figure 16: *Scaling of Reflected Radiative Green Functions with Cloud Parameters.* (a) Numerical values of root-mean-square (r.m.s.) horizontal photon transport in reflectance $\langle\rho^2\rangle_R^{1/2}$ divided by the r.h.s. of Eqs. (21) or (23) plotted vs. rescaled optical depth $(1-g)\tau$ in Eq. (20). (b) Same as in (a) for mean photon path $\langle\lambda\rangle_R/\Delta_z$; note the need here for a significant pre-asymptotic correction term introduced in Eq. (24).

5.2 Extra-Stretch in LITE's Pulses

The δ-illumination can be pulsed, as in a high-power laser, rather than steady; accordingly, we envision a space-time radiative Green function. Standard atmospheric lidar probing exploits a small sub-sample of the entire remotely-observable space-time Green function. In the true spirit of radar, only the return along the transmitted beam is used, and the optical "echo" is interpreted as a single back-scattering event. To facilitate this interpretation, the angular aperture of the lidar detector is generally made almost as small as the divergence of the transmitted beam ($\approx 10^{-3}$ rad).

In Sept. 1994, the first space-borne lidar system was flown on Space Shuttle Discovery during the Lidar-In-space Technology Experiment (LITE). Its specifications were not too different from ground-based and air-borne systems:[83] beam divergence = day-time field-of-view (FOV) = 1.1 mrad, and night-time FOV = 3.5 mrad. Only, from a range of ≈ 260 km, this leads to a beam 290 m in diameter at cloud-level, and angular integration over an area 920 m in diameter. This means that virtually the whole "spot" in Fig. 15b is incorporated, hence all orders-of-scattering rather than a single one. In the conventional interpretation of lidar signals, total photon path λ (return-time converted to distance) is a measure of range from the instrument, $\lambda/2$; when dense low-altitude (≈ 1 km) marine Sc were being probed, LITE's geometry places the origin of the echo for the most highly scattered photons well below sea-level. MC simulation of the temporal Green function in Fig. 15d demonstrates how easily this (amount of pulse-stretching) can occur.[84]

Figure 16b is the temporal (photon path) counterpart of Fig. 16a, showing mean total path $\langle \lambda \rangle_R$ plotted versus $(1-g)\tau$ for reflection from fractal and homogeneous cloud models. These numerics can be encapsulated into

$$\langle \lambda \rangle_R \approx \Delta_z \times \{ \ 1 + correction(g, \langle \tau \rangle) \ \}, \tag{24}$$

bearing in mind that the distribution of photon paths is quite broad and negatively skewed. Indeed, a large portion of the photons are reflected after rather short paths (just a few scatterings), but some of them wander almost to the opposite side of the cloud before wandering back (typically every other photon is transmitted).

5.3 Photon Diffusion Phenomenology: The Fractal Theory of Finite Random Walks

Clearly, there is a unique physical explanation for the solar phenomenon of radiative smoothing (manifested in the LANDSAT scale-break) and the lidar phenomenon of pulse-stretching in marine Sc (observed during LITE): photons are executing random walks, starting and ending at cloud boundaries. Equivalently, radiative transfer is in a diffusion regime , associated with so-called "asymptotic" theory.[91] This is not news to cloud-radiation instrumentalists: deep inside Sc, the angular distribution of radiance has the characteristic "monopole+dipole" structure of diffusion theory.[85] Why diffusion theory seems to work so well for the bulk properties of real clouds — with internal variability and (sometimes quite extensive) boundary layers included — is still somewhat of a mystery. As theoreticians of cloud-radiation interaction, we welcome this simplification (over kinetic theory). For example, the important formulas in Eqs. (23–24) can be derived analytically, including correction terms, in the homogeneous case from the closed-form solution of the nonstationary diffusion equation with the appropriate boundary conditions.[86]

The fractal properties of random walks provide considerable insight into diffusive cloud-radiation processes. To demonstrate this, we can derive the leading terms in Eqs. (23–24) and their counterparts for transmittance from first principles following closely the scaling arguments

used in ref. [87]. Assume all the photons are released isotropically into 3D space from the origin at time $t = 0$; then [14]

$$\langle r^2 \rangle = Dt \qquad (25a)$$

where

$$D = cl_t \qquad (25b)$$

is radiative diffusivity, c being the velocity of light. Now $r^2 = \rho^2 + z^2$ and the random walks are actually confined to the slab $0 \leq z \leq \Delta_z$. The easiest statistics to obtain are for transmitted photons: isotropy requires $\langle \rho^2 \rangle_T = 2\langle z^2 \rangle$ hence, at $z = \Delta_z$,

$$\langle \rho^2 \rangle_T^{1/2} \approx \Delta_z. \qquad (26)$$

In analogy with our investigation of the structure of reflected radiation fields, this will be the characteristic smoothing scale "η_T" for radiation transmitted through horizontally variable clouds. Next, we derive transit time through the slab: $\langle r^2 \rangle = 3\langle z^2 \rangle$ by isotropy hence, at $z = \Delta_z$, we have $\langle t \rangle_T \approx \Delta_z^2/D$; equivalently, for photon path $\lambda = ct$, we obtain

$$\langle \lambda \rangle_T \approx \Delta_z^2/l_t. \qquad (27)$$

Reflectance statistics follow from there. The graph dimension of $z(t)$, standard Brownian motion, is[21] $D_g = 2 - H_1 = 3/2$, hence the fractal dimension of its zero-crossing set,

$$D_z = \max\{D_g - 1, 0\} = 1/2. \qquad (28a)$$

The standard probabilistic interpretation of this geometrical statement is that, if t_r is the first "return-to-origin" time for an *unbounded* realization of $z(t)$, then[14]

$$\text{Prob}_\infty\{t_r \geq t\} = \int_t^\infty dP_\infty(t_r) \sim (ct/l_t)^{-D_z}, \qquad (28b)$$

where subscript "∞" reminds us that this applies to a semi-infinite optical medium. Combining Eqs. (27–28) immediately tells us that transmission probability[*] $T \approx \text{Prob}_\infty\{t_r \geq \langle t \rangle_T\}$ is proportional to $(\langle \lambda \rangle_T/l_t)^{-1/2} = (\Delta_z/l_t)^{-1} = [(1-g)\tau]^{-1}$, as seen in Fig. 11a for large optical depth and $\varpi_0 = 1$. Next, we find $\langle t \rangle_R$ by truncating the divergent distribution in Eqs. (28a–b) at $\langle t \rangle_T$:

$$\langle t \rangle_R = \int_0^\infty t dP_{\Delta_z}(t) \approx \int_0^{\langle t \rangle_T} t_r dP_\infty(t_r) \sim (c/l_t)^{-1/2}\langle t \rangle_T^{1/2} = \Delta_z/c, \qquad (29)$$

where subscript "Δ_z" designates a PDF for an optical medium of finite thickness. This leads to Eq. (24) for photon path. Equation (23) for spot-size follows from Eqs. (25a–b) and (29), once again projected onto the horizontal plane.

---

[*]A variant of this argument for Lévy-stable steps[56] requires an interesting refinement of the crucial statistical interpretation of D_z in Eq. (28a).

5.4 Off-Beam Cloud Lidar: A New Application of an Old Idea

The main difference between the conceptual models for (standard) atmospheric lidar and weather radar signals is that the former suffers from attenuation along the beam in both directions by scattering/absorbing processes. In fact the associated two-way exponential transmission term makes the signal almost undetectable at a range corresponding to 2–3 photon MFPs. Consequently, lidar beams do not penetrate clouds much thicker than cirrus layers that occur in the upper troposphere. The only useful information lidars deliver for dense boundary-layer clouds is their height ("cielometry") and an indication of the thermodynamic phase of water at cloud base. However, at most wavelengths of interest here (0.5–1.0 μm) the laser photons are not absorbed but scattered out[†] of the beam. This means that these photons are not lost but feed the diffuse radiation field in the cloud that we have described in the above sections as its Green function. Furthermore, these diffusing photons are detectable by emerging "off-beam" lidar techniques.[81]

Equations (23–24) tell us that a lidar system with off-beam imaging or, at least, spot profiling capabilities as well as the usual time-binning can be used to retrieve simultaneously cloud thickness (Δ_z) and density (from τ or l_t), given g. The naturally defined resolution of these measurements is about a spot-diameter, namely, 0.5 km under typical conditions. In essence, this is a direct application of diffusing-wave spectroscopy (DWS) to cloud structure. DWS is a very promising non-intrusive medical imaging technique[89] for locating, say, aneurysms (i.e., absorbing anomalies) in brain tissue, which is highly scattering. The difference is that size, shape and position of the absorbing entities are unknown in medical DWS and here we are dealing only with the unknown position of the (absorbing) cloud boundary opposite to the photon source. On the other hand, multiple source/detector positions can be used in the biological application.

The idea of obtaining information about the structure and composition of a system by irradiating it with particles or waves is of course not new. It is interesting however that such a standard laboratory procedure is now becoming available in the most readily accessible laboratory for strongly nonlinear phenomena: the Earth's atmosphere.

6. SUMMARY, DISCUSSION AND OUTLOOK

We have surveyed the last five years of work on multifractal data analysis, fractal cloud modeling, and cloud-radiation interaction theory at NASA's Goddard Space Flight Center.

Fractal theory:

- "bounded" cascade models,[42] a nonstationary 2-parameter generalization of Meneveau and Sreenivasan's "*p*-models" for the intermittent dissipation rate field in turbulence (cf. ref. [20]);
- having $\zeta(q) = \min\{qH,1\}$ independently of p (derived by renormalization), bounded cascades undergo a 1st-order multifractal phase transition at critical "temperature" $1/q_c = H > 0$;[26]

Data analysis:

- operational criteria, applicable to scale-invariant (regimes in) geophysical datasets, for detecting *bone fide* nonstationarity[9,13] and intermittency,[32] as opposed to their spurious counterparts that are merely symptoms of limited sampling (i.e., range of scales, and variety of events);

[†]Because atmospheric particles tend to scatter strongly into the forward direction, the single-scattering lidar equation is often corrected for multiple small-angle scatterings where the photons never leave the finite-sized beam.[88]

- "bi-fractal" analysis, a simple and robust two-exponent characterization of scale-invariant data as an improved diagnostic device with respect to stand-alone spectral analysis;[8,10]

Cloud structure:

- uncovering the bi-fractal universality of internal boundary-layer cloud structure with respect to the local climatic regime, and significant differences in higher-order statistical properties;[10,11]
- confirmation of the non-Poissonian nature of the spatial distribution of cloud droplets at small (sub-m) scales in records of *in situ* liquid water content at unprecedented 4-cm resolution;[11]

Radiative transfer theory in clouds:

- formal definition of the "Independent Pixel" (IP) approximation[42] as a simple approach to 3D radiative transfer applicable to fractal clouds in both simulation and retrieval modes;[38,76]
- confirmation of photon diffusion as the primary mode of solar[72,76] and lidar[81,87] radiation transport in boundary-layer clouds;
- utilization of the fractal geometry of the truncated random walks of photons in clouds to quantify their lateral diffusion in the process of "radiative smoothing;"[87]
- identification of radiative "channeling" patterns as the elementary perturbation of photon flow by spatial variability in the cloud;[76]

Large-scale cloud-radiation interaction in solar/near-IR spectrum (relevant to climate studies):

- mean-field parameterization, within the IP approximation, of the effect on planetary albedo of sub-grid variability in stratus clouds using variance of the log of local optical depth;[42,58]
- negative result in attempting to explain with 3D radiation transport effects recent observations of enhanced column absorption in presence of clouds at solar/near-IR wavelengths;[67]

Small-scale cloud-radiation interaction in solar spectrum (relevant to remote-sensing studies):

- estimation of the averaging required in energy budget (hence absorption) computations for the atmospheric column to balance the effect of fractal variability in an embedded cloud layer;[74]
- application of spectral[71] and multifractal[38] statistics to the quantitative assessment of the verisimilitude of the IP approximation in cloud remote-sensing studies;
- tracing the scale-breaking mechanism in LANDSAT cloud scenes (30-m resolution) to radiative smoothing, and it interpretation as the break-down of the IPA at 0.2–0.4 km scales;[38,72]
- temporal counterpart of the spatial smoothing of LANDSAT radiance fields found in the extra-stretch of laser pulses returned to the Shuttle-based Lidar-In-space Technology Experiment;[72]

New applications of radiative Green functions:

- improvement of direct[38] (and inverse[82]) IP approximations at scales normally contaminated by radiative smoothing by convolutions (or deconvolutions) of IPs with radiative Green functions;
- scaling properties of spatial and temporal radiative Green functions used to design a new type of cloud lidar based on multiple (rather than single) scattering theory.[81,86–87]

In each of the above exercises, the fractal nature of internal cloud structure — both apparent (in radiation fields) and inherent (*in situ* probing) — is highlighted in data and/or used in modeling. In particular, fractal cloud models play a central role in the design and implementation of

meteorological "Observation Simulation Systems," i.e., computational tools that model hypothetical or real observational procedures end-to-end.[67,74,81] Even if simpler-to-understand homogeneous cloud models are used, fractality reappears at the heart of the radiative transfer process: in the convoluted geometry of photon paths shaped by random scattering events.[38,72,87]

Apart from the worthwhile pursuit of the last two items in the above list, we will apply in the near future the same general strategy (data analysis → cloud modeling → radiation computations) to more complex cloud types: e.g., broken cloud fields and multi-layered cloud systems. We will start with more intricate 2D and 3D data, based primarily on the new technology of millimeter (cloud droplet) radar, and apply more powerful and robust analysis methods using wavelet transforms.[29,45] Having developed the methodology for injecting "real" atmospheric optics into fractal cloud models, we can address the two other standard critiques of fractal cloud modeling by mainstream meteorologists: lack of dynamics, lack of thermodynamics. One way of injecting some thermal physics, replete with phase transitions, into fractal models is to use the fractal field — still a surrogate for the 3D fluid dynamics — as a stochastic forcing term in 1D cloud models based on (so-called "air-parcel") theory of adiabatic ascent. Preliminary attempts in this direction show a richer structure than the purely stochastic models, including gaps (of widely variable sizes) between cloudy portions.

After stimulating the creativity of artists, poets, even musicians for millennia, those complex hydro-thermodynamical atmospheric phenomena we call "clouds" became one of the earliest motivations in the development of fractal geometry. And that was only our subjective visual impression of clouds. They have since become the focus of intense objective scrutiny with scientific instruments ranging from simple hygrometers on balloons to accurately calibrated radiometers on satellites to sophisticated new radar and lidar systems. And the data harvested from these instruments is now spurring some necessary refinements in fractal science. Indeed, the first four entries in the above list of achievements are purposefully not specific to cloud science. This is to say that the problems of statistical data analysis and stochastic modeling posed by clouds (from the radaitive perspective alone) are not always amenable to existing techniques.

In summary, we do not perceive cloud structural and radiation studies as outlets for *ab initio* fractal ideas. Scale-breaks, limited scaling ranges, limited amounts of data, and the healthy level skepticism prevailing in the meteorological community being "serviced" are a constant challenge to fractal scientists dealing with atmospheric phenomena, including the present authors. For support, we naturally turn to colleagues working in other areas, where fractals are presumably well-established. Our impression, formed at a number of interdisciplinary meetings, is one of an incredibly dynamic community grappling with its own growth. Maturation is imminent, and apparently somewhat painful. In our opinion, fractal science urgently needs to steer further away from its youthful and enthusiastic agenda in a descriptive geometrical "theory-of-everything" towards a stronger affiliation with statistical physics, i.e., critical phenomena, self-organization, thermodynamics, renormalization methods, (broken) symmetry, etc. Furthermore, it would be timely to secure the foundations of random fractal theory in terms of mathematical statistics, sampling and ergodic theories in particular. We hope that clouds, and the scientific challenges they pose in climate and remote-sensing, will continue to inspire the field of fractals-at-large in return for the progress fractals and multifractals have enabled in atmospheric science.

ACKNOWLEDGMENTS

providing the PVM-100A data from SOCEX. We thank Drs. A. Arking, A. Arnéodo, D. Avnir, B. Baker, H. Barker, T. Bell, R. Cess, R. Davies, F. Evans, P. Gabriel, M. King, S. Lovejoy, H. Melfi, K. Musgrave, J.-F. Muzy, R. Pierrehumbert, R. Pincus, S. Platnik, G. Pomraning, W. Ridgway, S. Roux, D. Schertzer, G. Stephens, G. Titov, S.-C. Tsay, D. Veneziano, J. Weinman among others at "Code 913" and elsewhere for many a fruitful discussion. AD is grateful for his lidar apprenticeship with Drs. P. Flamant, M. McGill, J. Pelon, J. Spinhirne, and D. Winker.

REFERENCES

1. Washington Advisory Group, *An Evaluation of the Atmospheric Radiation Measurement Program* (U.S. Department of Energy, Washington, DC, 1997).
2. R. F. Voss, in *Fundamental Algorithms for Computer Graphics*, p. 805, eds. Earnshaw *et al.* (Springer-Verlag, Berlin, 1985).
3. S. Lovejoy, *Science* **216** (1982) 185.
4. V. K. Gupta and E. C. Waymire, *J. Appl. Meteor.* **32** (1993) 251.
5. D. Ebert, K. Musgrave, P. Peachey, K. Perlin and S. Worley, *Texturing and Modeling: A Procedural Approach* (AP Professional, Orlando, FL, 1994).
6. Ch. Baudelaire, "La Soupe et les Nuages" (Petits Poème en Prose, No. XLIV) in *Spleen de Paris,* in *Oeuvres Complètes,* vol. IV (Marcel Lévy, Paris, 1869).
7. H. Gerber, B. G. Arends and A. S. Ackerman, *Atmos. Res.* **31** (1994) 235.
8. A. Davis, A. Marshak, W.J. Wiscombe and R.F. Cahalan, *J. Geophys. Res.* **D99** (1994) 8055.
9. A. Davis, A. Marshak, W.J. Wiscombe and R.F. Cahalan, *J. Atmos. Sci.* **53** (1996) 1538.
10. A. Marshak, A. Davis, W. J. Wiscombe, and R. F. Cahalan, *J. Atmos. Sci* **54** (1997) 1423.
11. A. Davis, A. Marshak, H. Gerber and W. J. Wiscombe, Horizontal Structure of Marine Boundary-Layer Clouds at 4-cm Resolution: Scale Break at 2–5 m, Non-Poissonian Behavior at Small Scales, Multifractal Behavior at Large Scales, *J. Geophys. Res. – D* (1997) submitted.
12. B. Baker, *J. Atmos. Sci.* **49** (1992) 387.
13. A. Davis, A. Marshak and W.J. Wiscombe, in *Wavelets in Geophysics*, p. 249, eds. E. Foufoula-Georgiou and P. Kumar (Academic Press, San Diego, CA,1994).
14. B. B. Mandelbrot, *The Fractal Geometry of Nature* (Freeman & Co., San Fransisco, 1982).
15. F. Anselmet, Y. Gagne, E. J. Hopfinger and R. A. Antonia, *J. Fluid Mech.* **140** (1984) 63.
16. U. Frisch and G. Parisi, in *Turbulence and Predictability in Geophysical Fluid Dynamics*, p. 84, ed. M. Ghil, R. Benzi and G. Parisi (North-Holland, Amsterdam, 1985).
17. P. Grassberger, *Physics Letters* **97A** (1983) 227.
18. H. G. E. Hentschel and I. Procaccia, *Physica D* **8** (1983) 435.
19. T. C. Halsey *et al.*, *Phys. Rev.* **A33** (1986) 1141.
20. C. Meneveau and K. R. Sreenivasan, *Phys. Rev. Lett.* **59** (1987) 1424.
21. K. J. Falconer, *Fractal Geometry* (John Wiley, New York, 1990).
22. S. I. Vainshtein *et al.*, *Phys. Rev.* **E50** (1994) 1823.
23. A. N. Kolmogorov, *Doklady Akad. Nauk SSSR* **30** (1941) 299.
24. T. Viscek and A.-L. Barabási, *J. Phys. A: Math. Gen.* **24** (1991) L845.
25. U. Frisch, *Proc. Roy. Soc. London* **A434** (1991) 89.
26. A. Marshak, A. Davis, R. F. Cahalan and W. J. Wiscombe, *Phys. Rev.* **E49** (1994) 55.
27. Y. Tessier, S. Lovejoy and D. Schertzer, *J. Appl. Meteor.* **32** (1993) 223.
28. D. Hamburger (Lidar), O. Biham, and D. Avnir, *Phys. Rev.* **E53** (1996) 3342.
29. J.-F. Muzy, E. Bacry and A. Arnéodo, *Phys. Rev.* **E47** (1993) 875.
30. E. Aurell, U. Frisch, J. Lutsko and M. Vergassola, *J. Fluid Mech.* **238** (1992) 467.

31. M. Eneva, *Nonlinear Processes in Geophysics* **1** (1994) 182.
32. A. Davis, A. Marshak, W. J. Wiscombe and R. F. Cahalan, in *Current Topics in Nonstationary Analysis*, p. 97, eds. G. Treviño *et al.* (World-Scientific, Singapore, 1996).
33. A. N. Kolmogorov, *J. Fluid Mech.* **13** (1962) 82.
34. A. Obukhov, *J. Fluid Mech.* **13** (1962) 77.
35. D. Schertzer and S. Lovejoy, *J. Geophys. Res.* **D92** (1987) 9693.
35. A. Davis, A. Marshak, W. J. Wiscombe and R. F. Cahalan, *Fractals* **1** (1993) 560.
37. R. T. Pierrehumbert, *Geophys. Res. Lett.* **23** (1996) 1095.
38. A. Marshak, A. Davis, W.J. Wiscombe and R.F. Cahalan, *J. Geophys. Res.* **D100** (1995) 26247.
39. A.S. Monin and A.M. Yaglom, *Statistical Fluid Mechanics*, vol. 2 (MIT Press, Boston, 1975).
40. W. J. Wiscombe *et al.*, in *Proceedings of the 4th Atmospheric Radiation Measurement (ARM) Science Team Meeting*, p. 11 (U.S. Department of Energy, Washaington DC, 1995).
41. R. F. Cahalan *et al.*, in *Proceedings of 4th International Meeting on Statistical Climatology*, p. 28, ed. J. Sansom (New Zealand Meteorological Service, Wellington, N.Z., 1990).
42. R. F. Cahalan, *et al.*, *J. Atmos. Sci.* **51** (1994) 2434.
43. R. F. Cahalan and J. B. Snider, *Remote Sens. Environ.* **28** (1989) 95.
44. M. J. Fiegenbaum, M. H. Jensen and I. Procaccia, *Phys. Rev. Lett.* **57** (1986) 1503.
45. A. Arnéodo, E. Bacry and J.-F. Muzy, *Physica A* **213** (1995) 232.
46. P. Bak, *How Nature Works* (Copernicus / Springer-Verlag, New York, 1996).
47. G. A. Titov, Radiative Horizontal Transport and Absorption by Stratocumulus Clouds, *J. Atmos. Sci.* (1997) submitted.
48. J. Wilson, D. Schertzer and S. Lovejoy, in *Scaling, Fractals and Non-Linear Variability in Geophysics*, p. 185, eds. D. Schertzer and S. Lovejoy (Kluwer, Hingham, MASS, 1991).
49. K. Stamnes, S. Tsay, W. Wiscombe and K. Jayaweera, *Appl. Opt.* **27** (1988) 2502.
50. W. E. Meador and W. R. Weaver, *J. Atmos. Sci.* **37** (1980) 630.
51. G. L. Stephens, *J. Quant. Spectrosc. Radiat. Transfer* **36** (1986) 51.
52. K. F. Evans, *J. Atmos. Sci.* **50** (1993) 3111.
53. R. G. Giovanelli, *Aust. J. Phys.* **12** (1959) 164.
54. S. Lovejoy, A. Davis *et al.*, *J. Geophys. Res.* **D95** (1990) 11699.
55. K. Case and P. Zweifel, *Linear Transport Theory* (Addison-Wesley, Reading, MASS,1967).
56. A. Davis and A. Marshak, in *Fractal Frontiers*, p. 63, eds. M. M. Novak and T.G Dewey (World Scientific, Singapore, 1997).
57. R. F. Cahalan, *Nonlinear Processes in Geophysics* **1** (1994) 156.
58. M. Tiedke, *Mon. Wea. Rev.* **124** (1996) 745.
59. B. Wielicki and L. Parker, *J. Geophys. Res.* **D97** (1992) 12799.
60. R. D. Cess *et al.*, *Science* **267** (1995) 496.
61. V. Ramanathan *et al.*, *Science* **267** (1995) 499.
62. P. Pilewskie and F. P. Valero, *Science* **267** (1995) 1626.
63. F. Valero, A. Bucholtz, B. Bush, S. Pope, W. Collins, P. Flatau, A. Strawa and W. Gore, The Atmospheric Radiation Measurements Enhanced Shortwave Experiment (ARESE): Experimental and Data Details, *J. Geophys. Res. – D* (1997) submitted.
64. Z.-Q. Li, H. W. Barker and L. Moreau, *Nature* **376** (1995) 486.
65. D. G. Imre, E. H. Abramson and P. H. Daum, *J. Appl. Meteor.* **35** (1996) 1991.
66. A. Arking, M–D. Chou and W. L. Ridgway, *Geoph. Res. Lett.* **23** (1996) 829.
67. A. Marshak, A. Davis, W. J. Wiscombe, W. Ridgway, and R. F. Cahalan, Biases in Shortwave Column Absorption in the Presence of Fractal Clouds, *J. Climate* (1997) in press.
68. R. N. Byrne, R. C. Somerville and B. Subasilar, *J. Atmos. Sci.* **53** (1996) 878.

69. W. O'Hirok and C. Gautier, The Role of Three-Dimensional Clouds on Atmospheric Absorption, *J. Atmos. Sci.* (1997) submitted.

70. L. C. Henyey and J. L. Greenstein, *Astrophys. J.* **93** (1941) 70.

71. A. Marshak, A. Davis, W. J. Wiscombe and G. Titov, *Remote Sens. Environ.* **52** (1995) 72.

72. A. Davis, A. Marshak, R. F. Cahalan and W. J. Wiscombe, *J. Atmos. Sci.* **54** (1997) 241.

73. S. Lovejoy, D. Schertzer, P. Silas, Y. Tessier and D. Lavallée, *Ann. Geophysicae* **11** (1993) 119.

74. A. Marshak *et al.*, Inhomogeneity Effects on Cloud Shortwave Absorption Measurements: Two-aircraft simulations, *J. Geophys. Res. – D* (1997) in press.

75. A. Davis *et al.*, in *IRS'96: Current Problems in Atmospheric Radiation*, p. 809, eds. W. L. Smith and K. Stamnes (Deepak, Hampton, VA, 1997).

76. A. Davis, A. Marshak, R. F. Cahalan and W. J. Wiscombe, Insight into Three-Dimensional Radiation Transport Processes from Diffusion Theory, with Applications to the Atmosphere, in *Proc. of Int. Symp. on Radiative Transfer* (Begell House, New York, 1997) in press.

77. C.J. Cannon, *Astrophys. J.* **161** (1970) 255.

78. G. L. Stephens, *J. Atmos. Sci.* **45** (1988) 1836.

79. A. Davis, S. Lovejoy and D. Schertzer, *S.P.I.E. Proceedings*, **1558** (1991) 37.

80. A. Davis, *Radiation Transport in Scale-Invariant Optical Media*, PhD thesis (McGill University, Physics Department, Montreal, 1992).

81. A. Davis *et al.*, in *Proceedings of Winter Topical Meeting on "Optical Remote Sensing of the Atmosphere,"* p. 39 (Optical Society of America, Washington DC, 1997).

82. A. Marshak *et al.*, Nonlocal Independent Pixel Approximation: Direct and Inverse Problems, *IEEE Trans. Geosc. and Remote Sens.* (1997) in press.

83. D. M. Winker, R. H. Couch and M. P. McCormick, *Proc. IEEE* **84** (1996) 164.

84. D. M. Winker, in *Advances in Atmospheric Remote Sensing with Lidar*, p. 185, eds. A. Ansmann, R, Neuber, P. Rairoux and U. Wadinger (Springer-Verlag, Berlin, 1996).

85. M. D. King, L. F. Radke and P. V. Hobbs, *J. Atmos. Sci.* **47** (1990) 894.

86. A. Davis and A. Marshak, in *8th International Worskshop on MUltiple SCattering Lidar Experiments (MUSCLE 8) – Extended Abstract Volume*, p. 67 (DREV, Valcartier, Qc, 1996).

87. A. Davis *et al.*, in *Advances in Atmospheric Remote Sensing with Lidar*, p. 193, eds. A. Ansmann, R, Neuber, P. Rairoux and U. Wadinger (Springer-Verlag, Berlin, 1996).

88. C. Flesia and P. Schwendimann (eds.), Special section on MUltiple SCattering in Lidar Experiments (MUSCLE), *Applied Physics B – Lasers and Optics*, **B60** (1995) pp. 315–362.

89. A. Yodh and B. Chance, *Phys. Today* **48** (1995) No. 3, 34.

90. D. Deirmendjian, *Electromagnetic Scattering on Spherical Polydispersions* (Elsevier, New York, 1969).

91. H. C. van de Hulst, *Multiple Light Scattering: Table, Formulas, and Applications.* vol. 2 (Academic Press, San Diego, CA, 1980).

92. D. Schertzer and S. Lovejoy, *Nonlinear Variability in Geophysics* (World Scientific, Singapore, 1997) in press.

93. A. N. Tikhonov, *Solutions of Ill-Posed Problems* (Winston, New York, 1977).